Teel_Formation_pmag

April 12, 2016

Contents

1 Paleomagntism of the Teel Formation

1.1 Teel Volcanics Data Analysis

What follows is an analysis of the Ordovician-Silurian Teel Formation. Most samples are basalts of Hirnantian age taken from flows to the east of Khukh Davaa in 2014.

1.1.1 Import Modules

Write template file (no_code.tpl) so that when the notebook is converted to a latex (then pdf) it excludes the large code blocks. This requires an additional arguement when using nbconveter and also requires that adding tables of content term after the document begins; can also add author. Can't include examples here because they affect the file when in latex.

```
Overwriting no_code_latex.tplx
```

1.1.2 Sampling localities

Table of site locality coordeinates in WGS84. Exact stratigraphic positions are shown in main text; order of stratigraphic position is given in "stat_pos" column of table.

```
Out[2]:    er_citation_names er_location_name er_site_name  site_lat  site_lon  \
        0         This study          unknown          Z30  47.10038  95.37550
```

1	This study	unknown	Z31	47.10049	95.37604
2	This study	unknown	Z32	47.10094	95.37684
3	This study	unknown	Z33	47.10107	95.37705
4	This study	unknown	Z34	47.10111	95.37712
5	This study	unknown	Z35	47.10069	95.37747
6	This study	unknown	Z36	47.10221	95.37959
7	This study	unknown	Z37	47.10211	95.37971
8	This study	unknown	Z38	47.09855	95.38445
9	This study	unknown	Z39	47.09860	95.38467
10	This study	unknown	Z40	47.09859	95.38474
11	This study	unknown	Z41	47.10109	95.37744
12	This study	unknown	Z42	47.09577	95.38577
13	This study	unknown	Z43	47.09570	95.38638
14	This study	unknown	Z44	47.09571	95.38651
15	This study	unknown	Z45	47.09562	95.38676
16	This study	unknown	Z46	47.09563	95.38692
17	This study	unknown	Z47	47.09568	95.38727
18	This study	unknown	Z48	47.09570	95.38744
19	This study	unknown	Z49	47.09581	95.38747
20	This study	unknown	Z50	47.09575	95.38781
21	This study	unknown	Z51	47.09584	95.38802
22	This study	unknown	Z52	47.09583	95.38815
23	This study	unknown	Z53	47.09442	95.37205
24	This study	unknown	Z54	47.09502	95.37299
25	This study	unknown	Z55	47.09525	95.37351
26	This study	unknown	Z56	47.06403	95.42075
27	This study	unknown	Z57	47.06277	95.42039
28	This study	unknown	Z58	47.06277	95.42045

	strat_pos
0	4
1	5
2	6
3	7
4	8
5	9
6	11
7	12
8	13
9	14
10	15
11	10
12	16
13	17
14	18
15	19
16	20
17	21

18	22
19	23
20	24
21	25
22	26
23	1
24	2
25	3
26	27
27	28
28	29

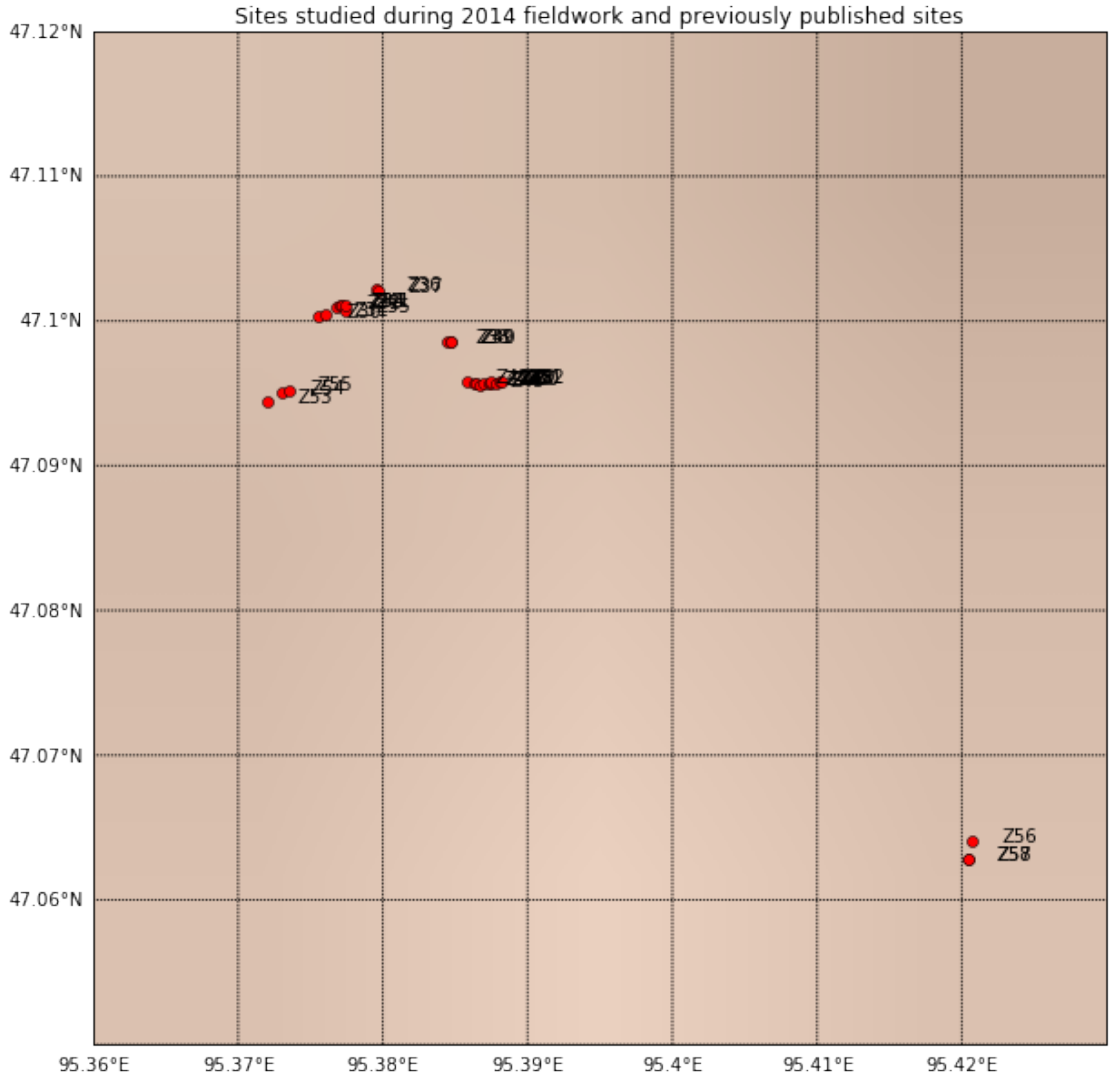

The paleomagnetic data from these sites may need to be tilt-corrected (given the age of magnetization) according to nearby measurements of bedding. The bedding measurements used for tilt-corrections are shown below.

Out[4]:

er_site_name	sample_bed_dip	sample_bed_dip_direction
Z30	58	88
Z31	58	88
Z32	55	84
Z33	55	84
Z34	55	84
Z35	55	84
Z36	47	89
Z37	47	89
Z38	46	87
Z39	46	87
Z40	46	87
Z41	55	84
Z42	37	87
Z43	37	87
Z44	37	87
Z45	37	87
Z46	37	87
Z47	37	87
Z48	28	91
Z49	28	91
Z50	28	91
Z51	28	91
Z52	28	91
Z53	58	88
Z54	58	88
Z55	58	88
Z56	24	165
Z57	24	165
Z58	24	165

The bedding measurements for flows Z56, Z57, and Z58 was measured from small lenses of sedimentary rocks between flows (**or from flow banding????**). We average these measurements by taking a fisher mean of the poles derived from the bedding plane measurements.

Out[6]:

```
{'alpha95': 11.477330440177056,
 'csd': 7.5069268730952095,
 'dec': 345.07072586523549,
 'inc': 66.37591972421707,
 'k': 116.42484465586055,
 'n': 3,
 'r': 2.9828215360225578}
```


Out[7]:

```
{'alpha95': 180.0,
 'csd': 75.717272007537375,
 'dec': 44.552429367843892,
 'inc': 50.036988188443182,
```

```
'k': 1.1444059858078446,
'n': 8,
'r': 1.8832895958171265}
```

For the first three measurements the bedding has as average So (strike/dip, right-hand rule) of 75/24, or DD-D (dip direction-dip) of 165-24. For all of the measurements there is an average bedding with an So of 104/24, or DD-D of 194-24.

We belief the first three bedding measurements are the most representative for the outcrop panel and are applied to the table above.

1.1.3 Principal-component analysis of data

Below we import paleomangetic results that were analyzed using demag_gui.py from the PmagPy python package. These are the vector component fits to all Teel sample data, including components from all temperature ranges.

We will go through each site, Z30 through Z58, and calculate site mean directions from vector fits of demagnetization data, including fits from all temperture ranges. Components have been classified according to their relative temperature ranges. 'LOW' components are typically below 200°C, 'MAG' refers to a temperature range within the unblocking range of magnetite (up to 580°C), 'HEM' refers to vector components fit to data points in the unblocking range of hematite (up to 680°C), and 'MID' refers to components with temperature ranges between 'LOW' and 'MAG'.

Z30 Site Z30 was sampled in a rhyolite at the base of the Teel Formation stratigraphic section.

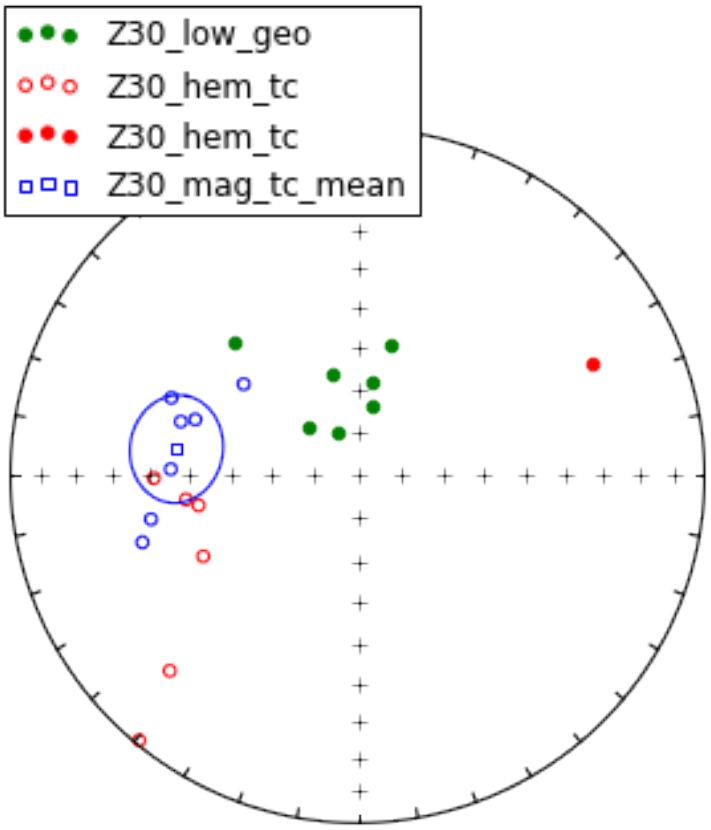

Z31 Only magnetite and low temperature, LOW (less than 200°C), components for Z31.

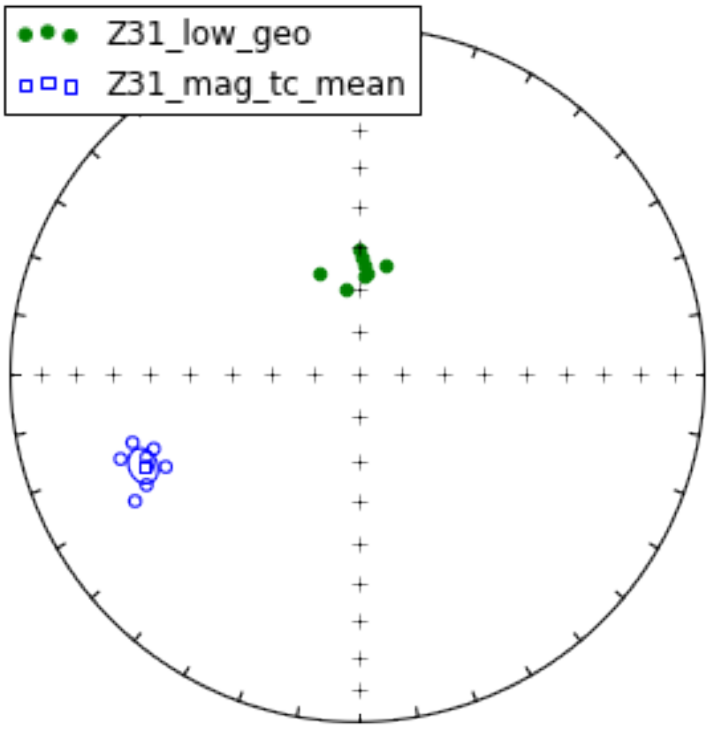

Z32 Only magnetite and low temperature, LOW (less than 200°C), components for Z32.

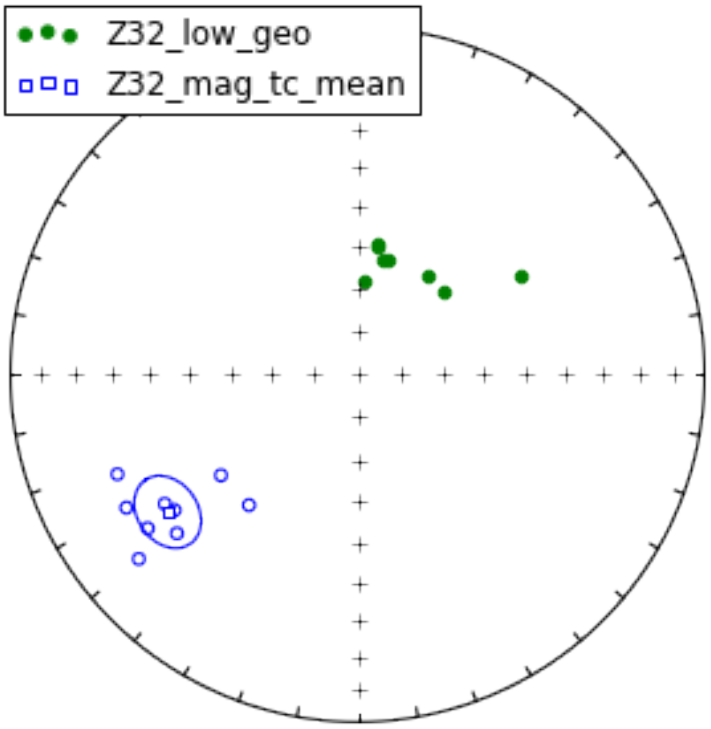

Z33 Only magnetite and low temperature, LOW (less than 200°C), components for Z33.

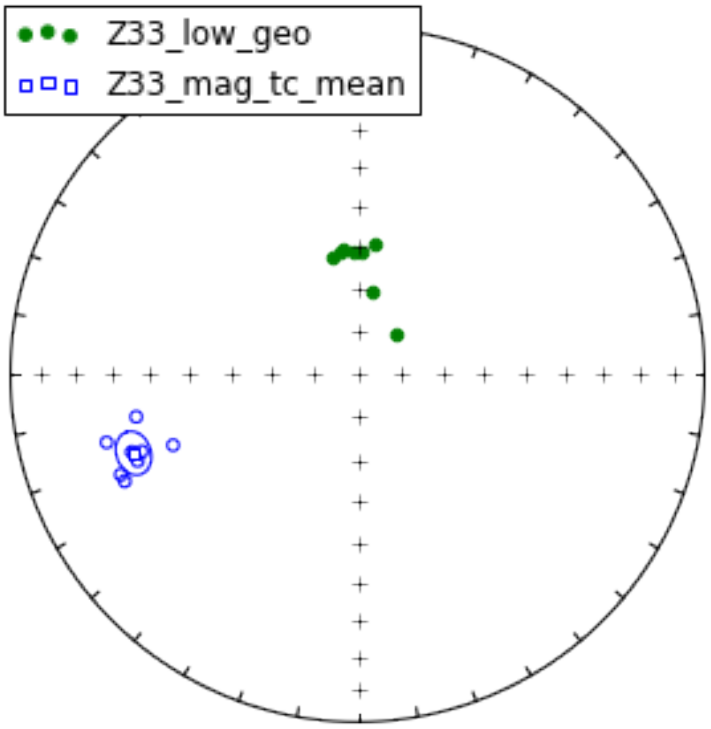

Z34 Only magnetite and low temperature, LOW (less than 200°C), components for Z34.

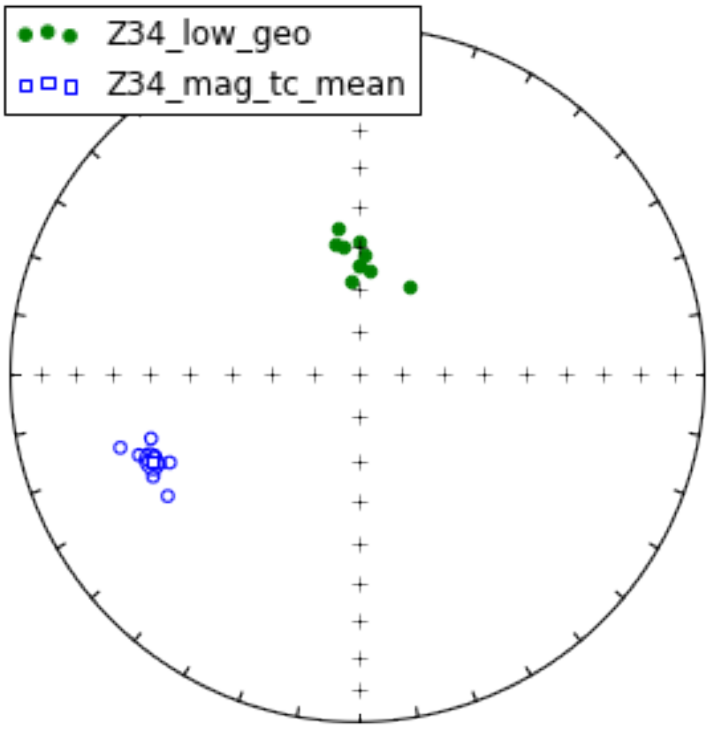

Z35 Hematite, magnetite, and low temperature, LOW (less than 200°C), components were calculated for Z35.

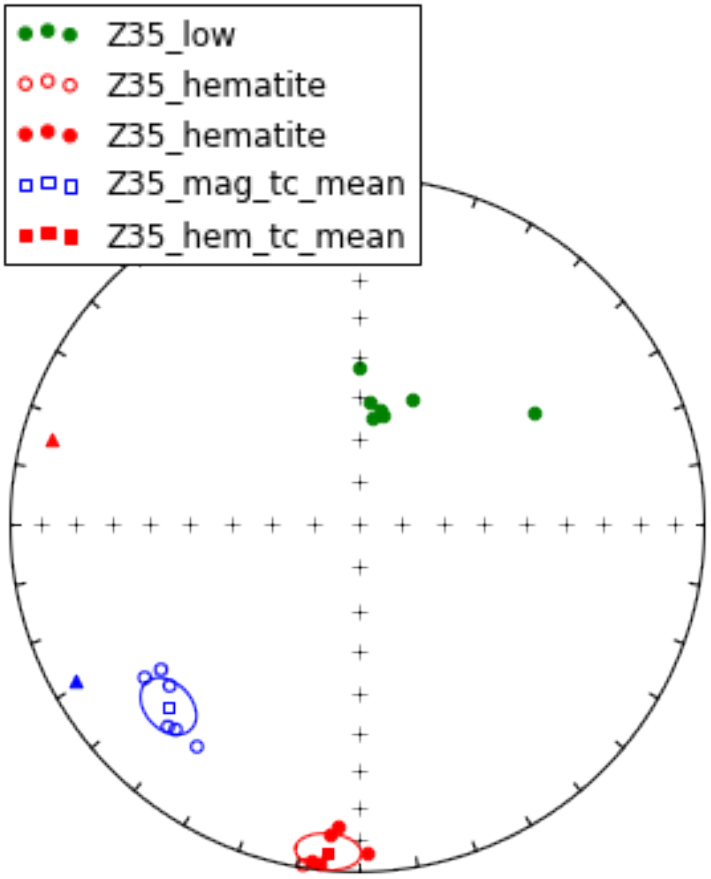

Data points shown with triangles were vectors from sample Z35.3 that were dropped from the mean calculation.

Z36 Only magnetite and low temperature, LOW (less than 200°C), components were calculated for Z36.

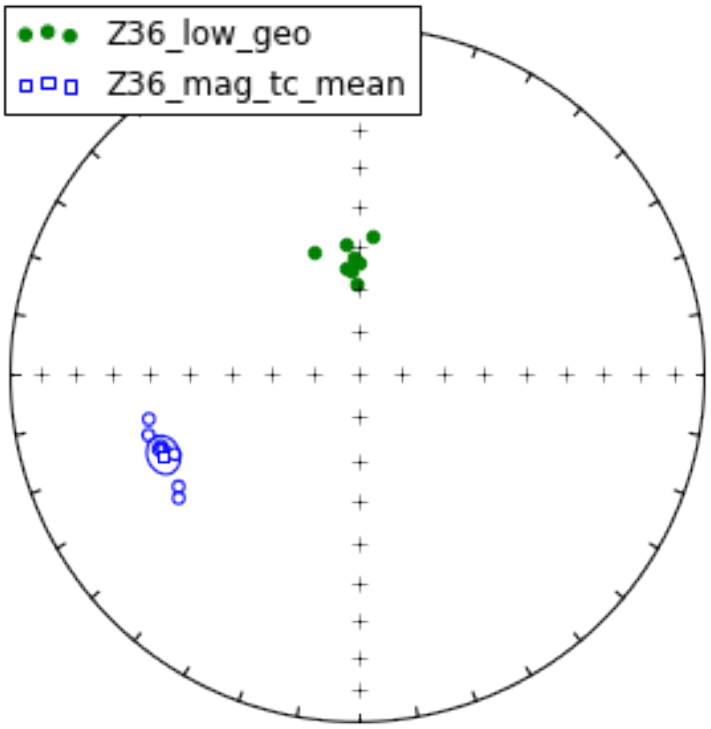

Magnetite and low temperature, LOW (less than 200°C), components were calculated for Z37.

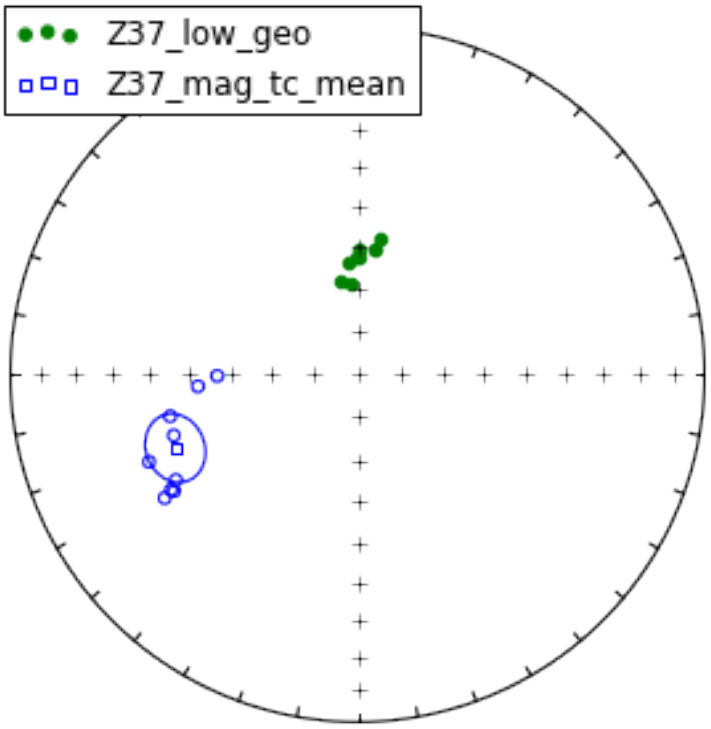

Z38 Hematite, magnetite, and low temperature, LOW (less than 200°C), components were calculated for Z38.

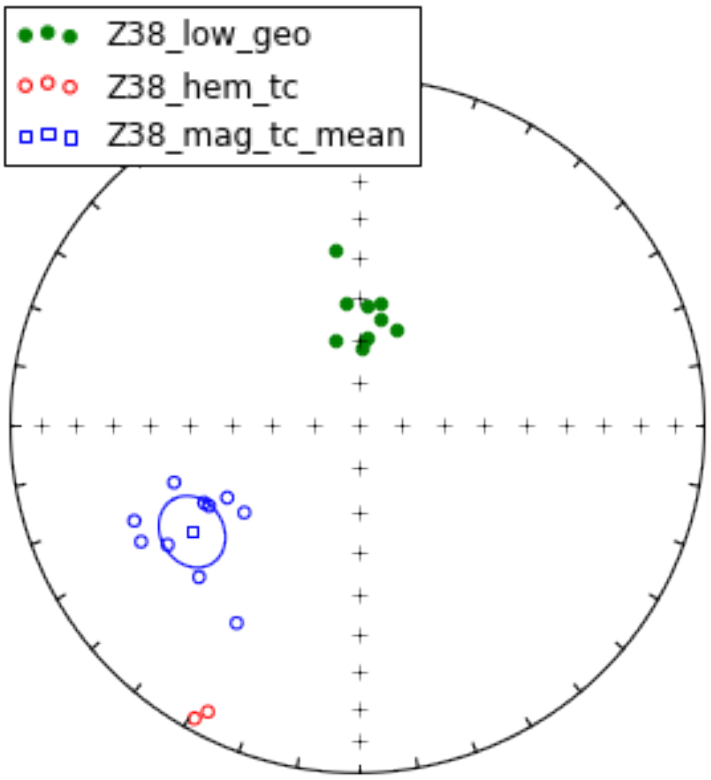

Only two samples yielded hematite components, therefore no mean was calculated for the hematite component.

Z39 Hematite, magnetite, and low temperature, LOW (less than 200°C), components were calculated for Z39.

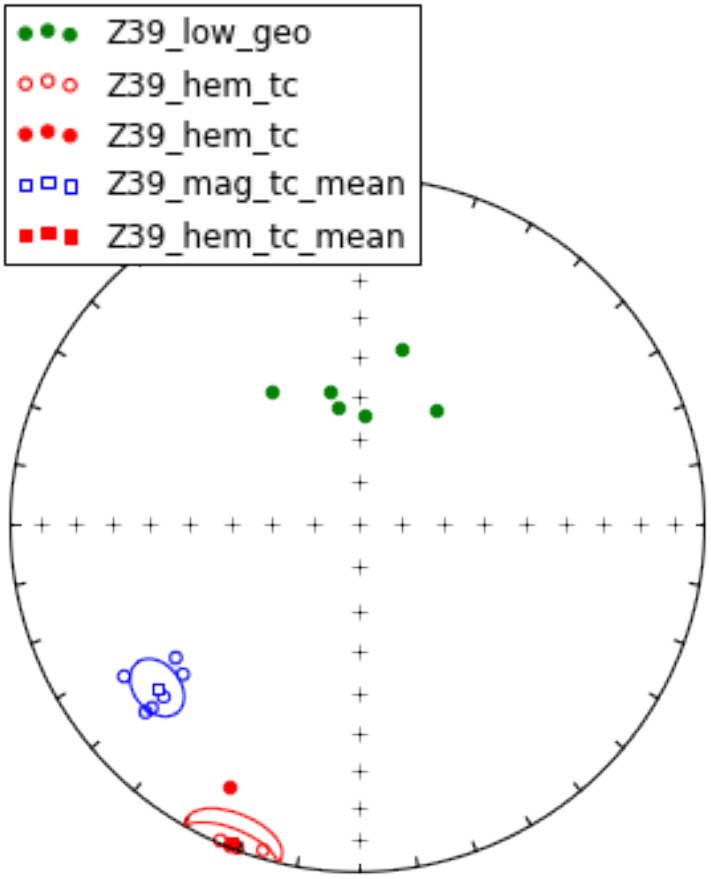

Z40 Hematite, magnetite, and low temperature, LOW (less than 200°C), components were calculated for Z40.

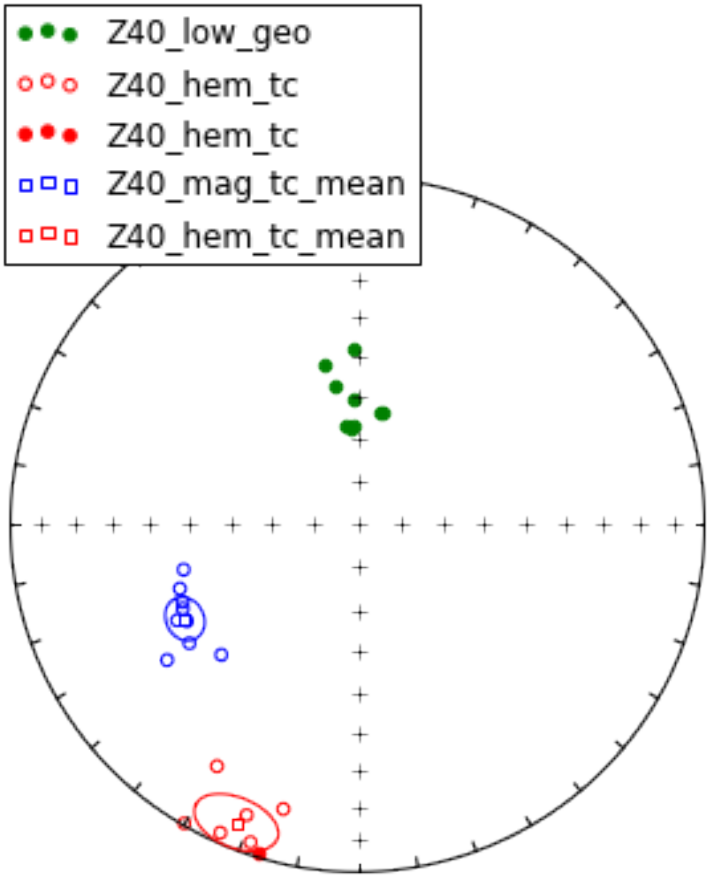

Z41

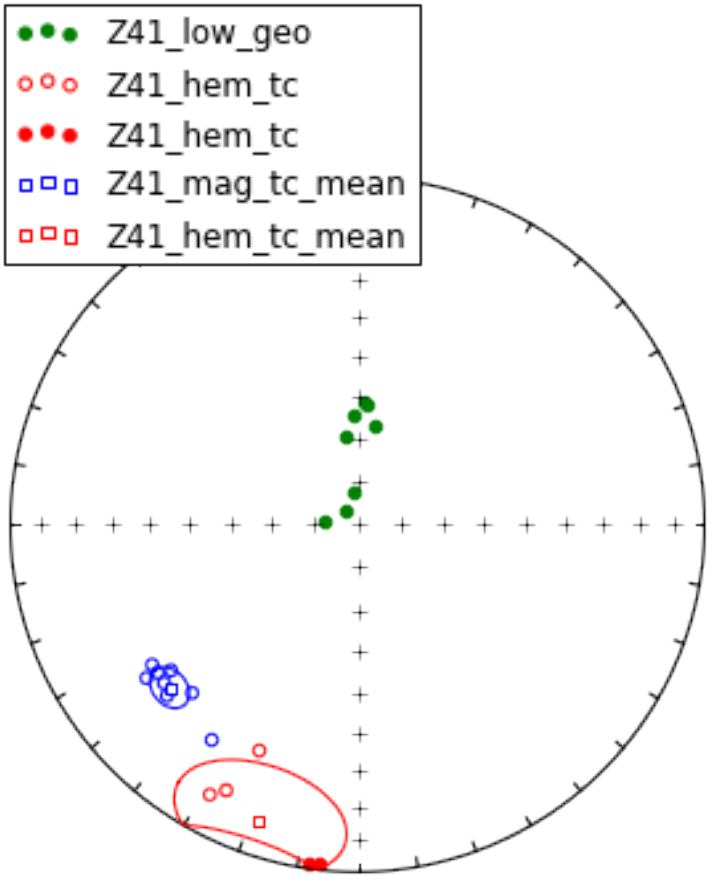

Z42 Hematite, magnetite, and low temperature, LOW (less than 200°C), components were calculated for Z42. A middle temperature component, MID, is also calculated, which derives from demagnetization steps between LOW and magnetite.

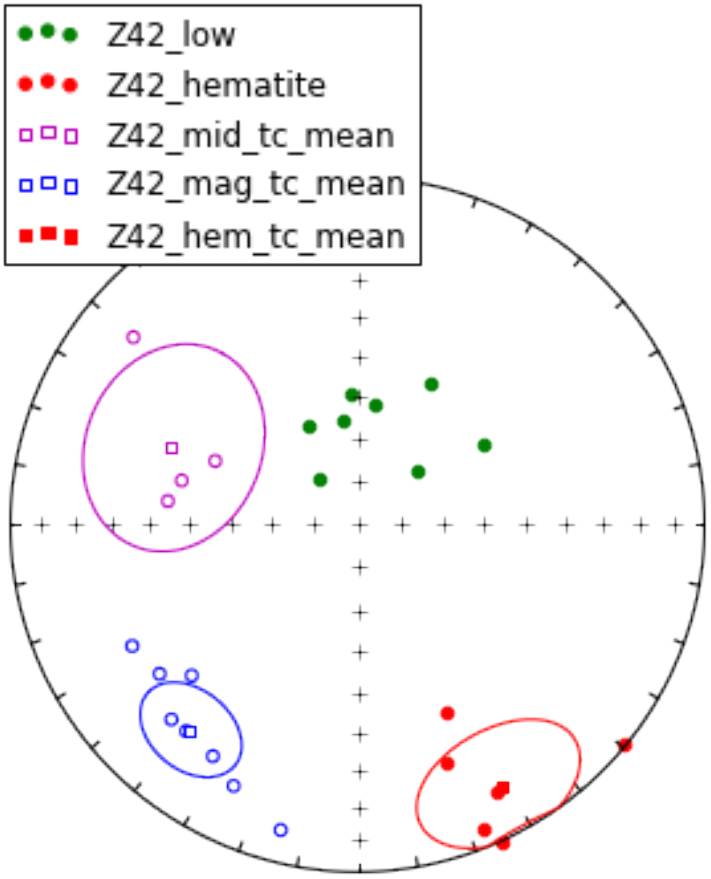

Z43 Hematite, magnetite, and low temperature, LOW (less than 200°C), components were calculated for Z43. A middle temperature component, MID, is also calculated, which derives from demagnetization steps between LOW and magnetite.

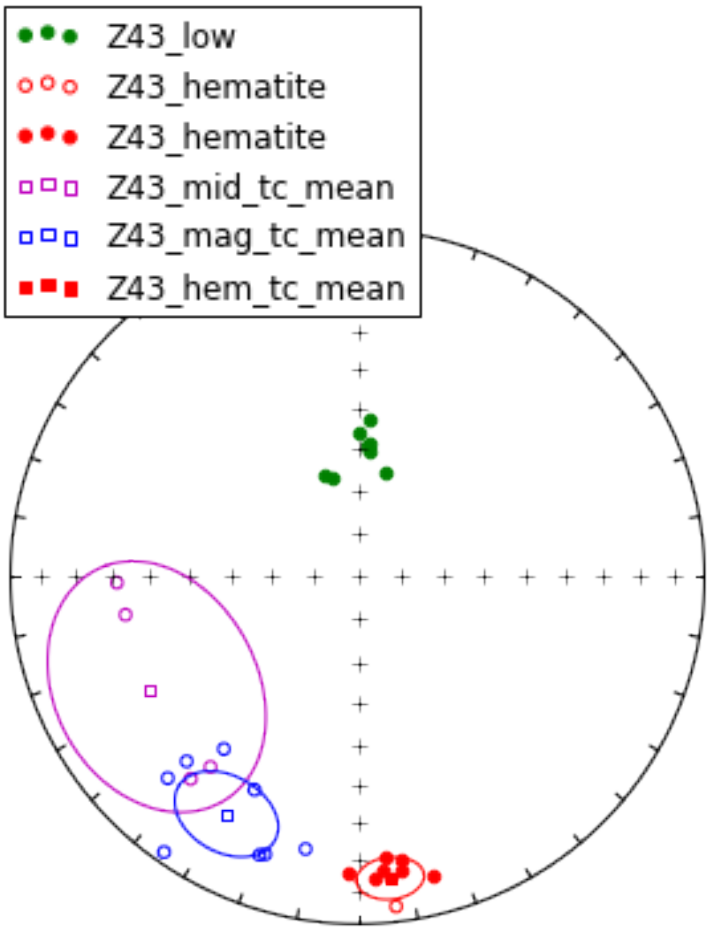

Z44 Hematite, magnetite, and low temperature, LOW (less than 200°C), components were calculated for Z44.

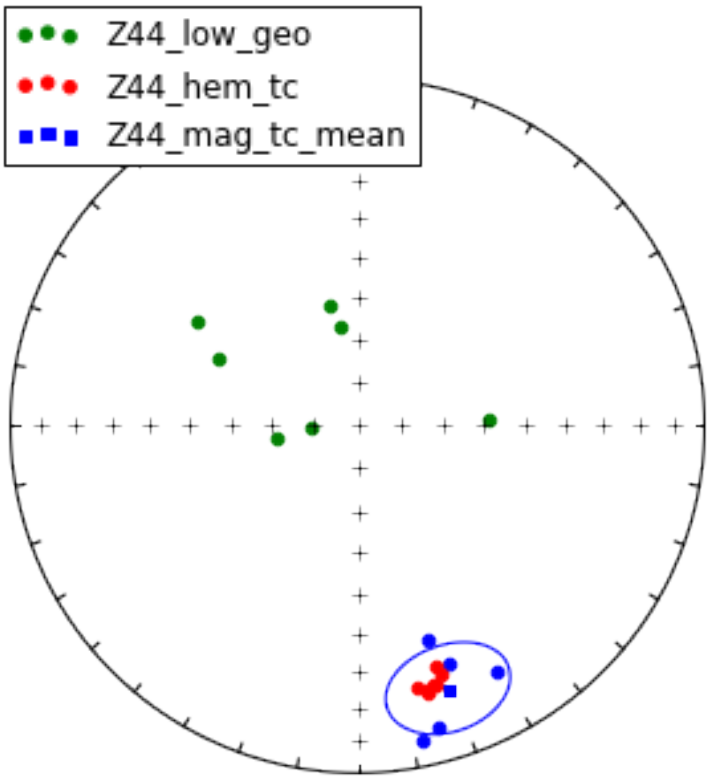

Z45 Hematite, magnetite, and low temperature, LOW (less than 200°C), components were calculated for Z45.

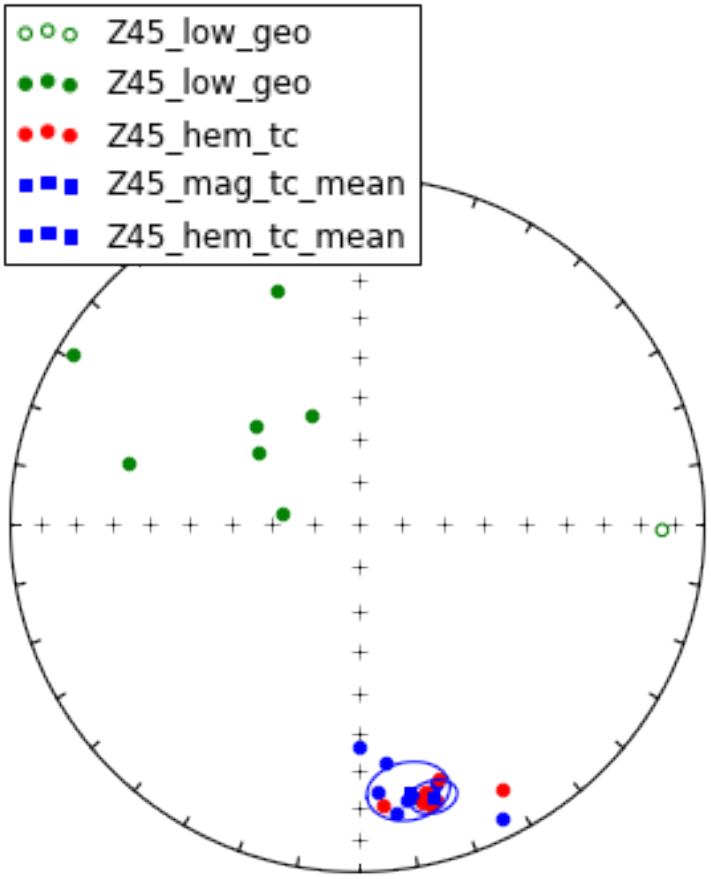

Z46 Hematite, magnetite, and low temperature, LOW (less than 200°C), components were calculated for Z46.

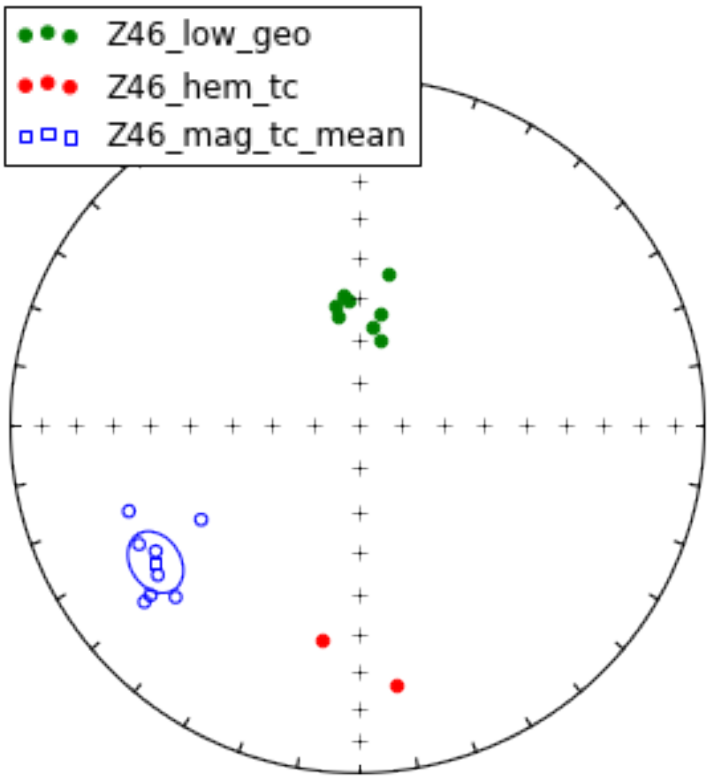

Z47 Hematite, magnetite, and low temperature, LOW (less than 200°C), components were calculated for Z47.

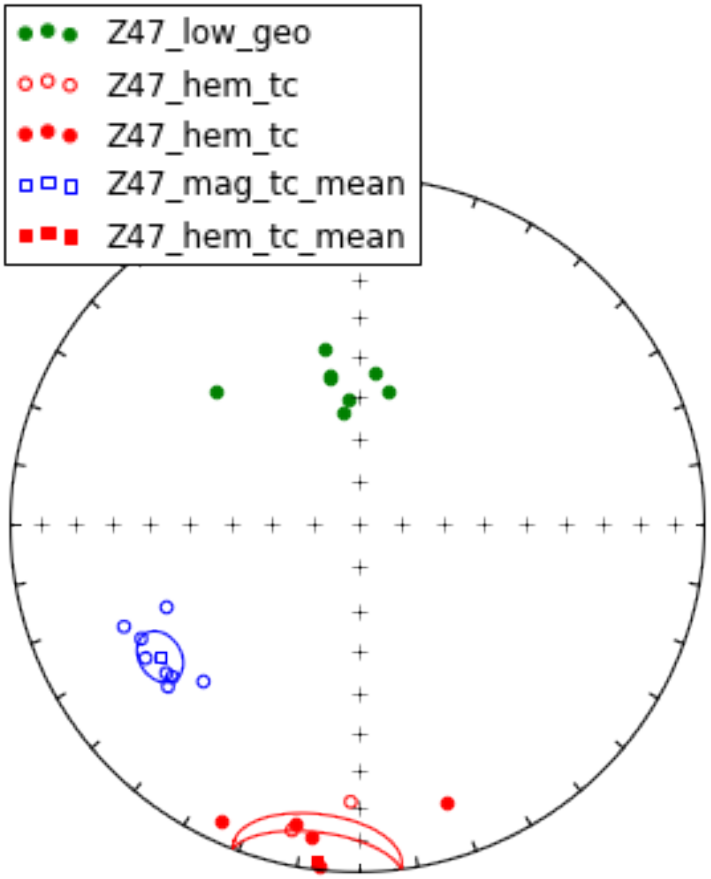

Z48 Hematite, magnetite, and low temperature, LOW (less than 200°C), components were calculated for Z48.

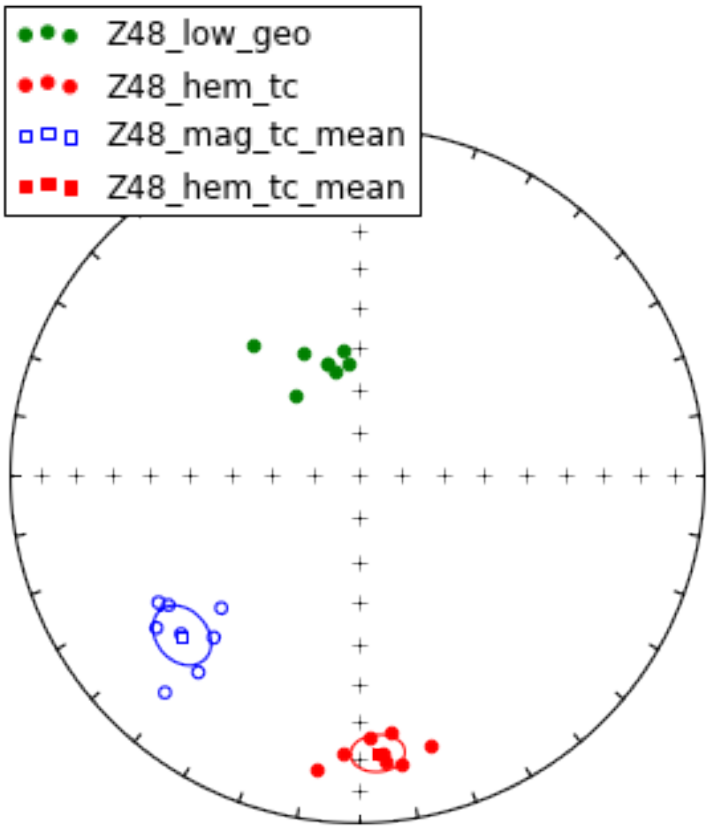

Z49 Hematite, magnetite, and low temperature, LOW (less than 200°C), components were calculated for Z49.

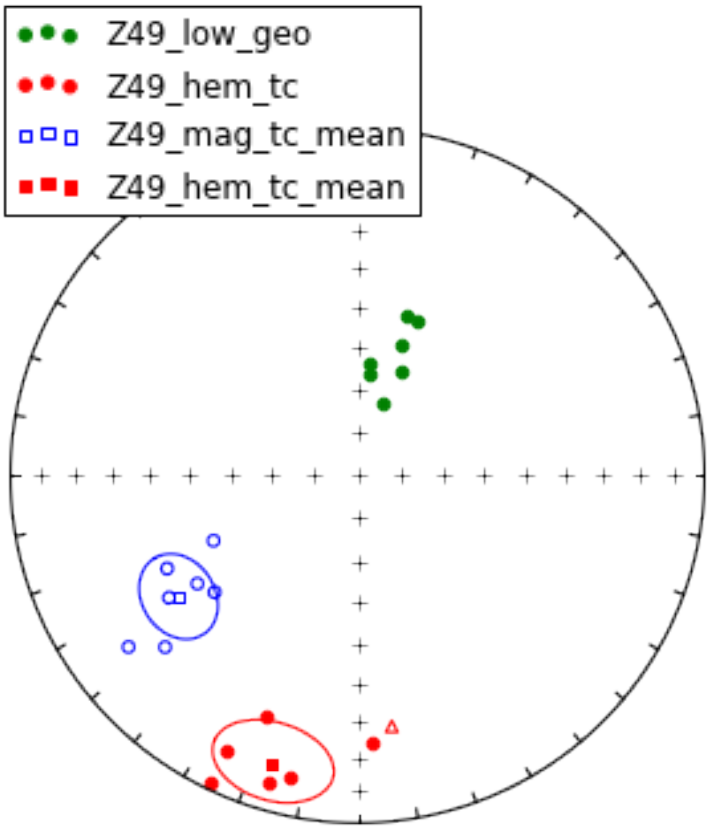

Z50 Only magnetite and hematite components could be distinguished from the demagnetization data or flow Z50.

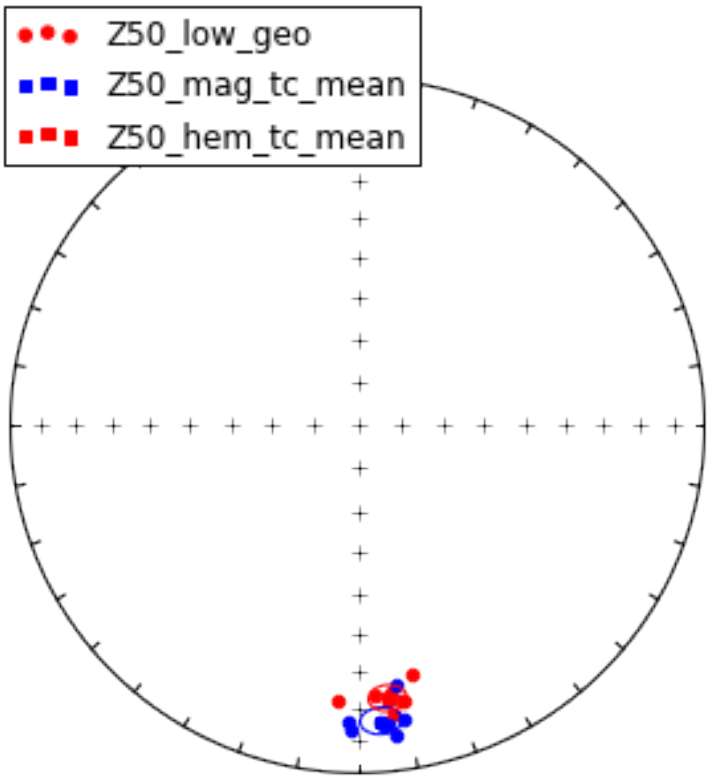

Z51 Hematite, magnetite, and low temperature, LOW (less than 200°C), components were calculated for Z51.

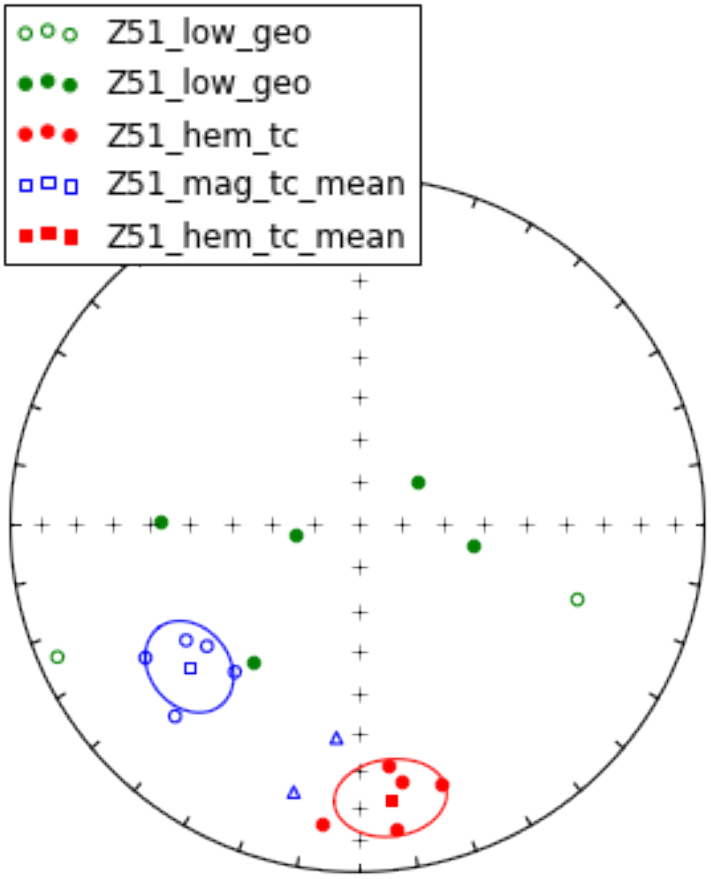

Magnetite components from two samples (Z51.1 and Z51.2) were excluded because of their similarity to hematite components (the hematite remanence mixed with that of magnetite) and different demagnetization behavior compared to the other magnetite components.

Z52 Hematite, magnetite, and low temperature, LOW (less than 200°C), components were calculated for Z52.

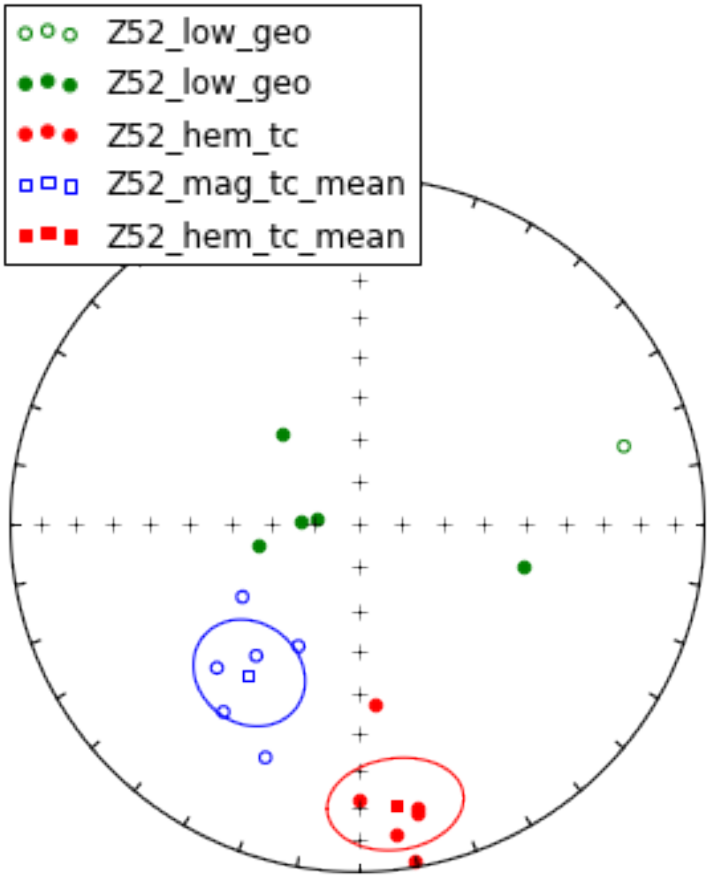

Z53 Hematite, magnetite, and low temperature, LOW (less than 200°C), components were calculated for Z53.

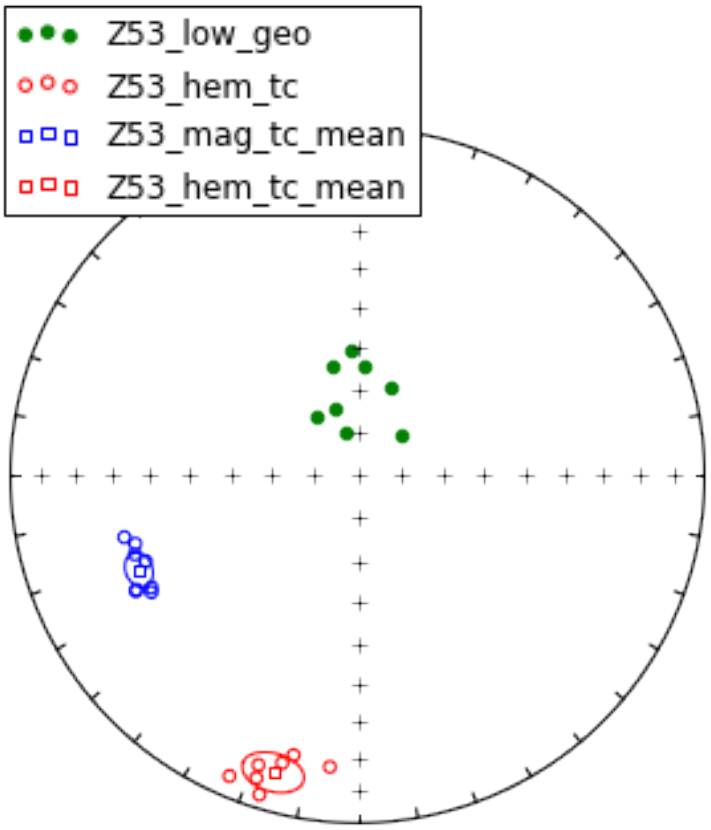

Z54 Hematite, magnetite, and low temperature, LOW (less than 200°C), components were calculated for Z54.

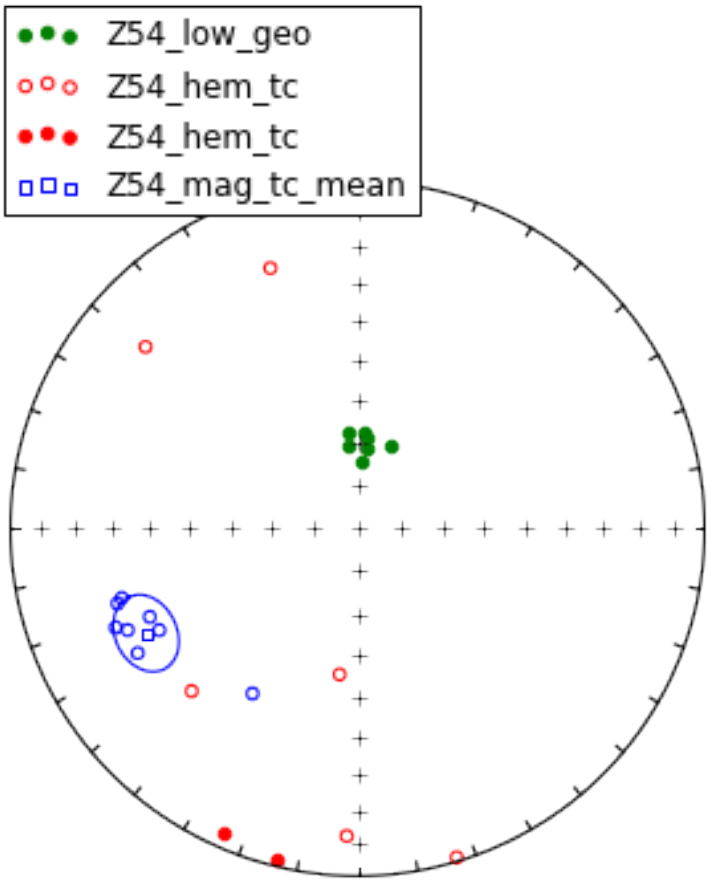

Z55 Magnetite and low-temperature, LOW (less than 200°C), components were calculated for Z55.

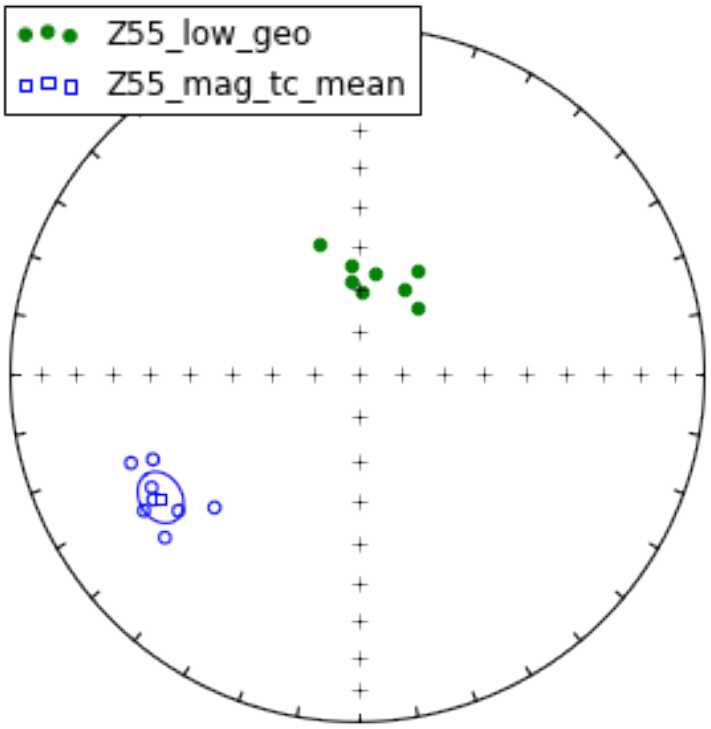

Z56 Hematite, magnetite, and low temperature, LOW (less than 200°C), components were calculated for Z56.

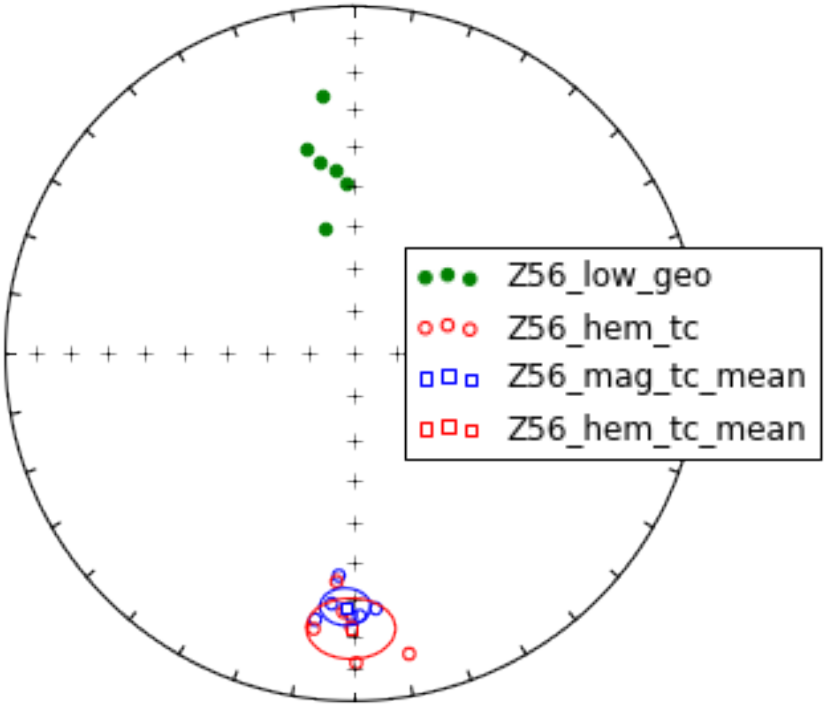

The directions from flow Z56 are very different from the rest of the sites. This may be due to the fact that these flows are from a different outcrop panel to the southeast of the majority of sites. The tilt correction for this panel may have led to these differences. It is also possible that the differences in directions is due to different (younger) age of flows Z56, Z57, and Z58. The magnetite and hematite components are the same, perhaps the result of overprinted magnetite that yield the same directions as hematite components.

Z57 Hematite, magnetite, and low temperature, LOW (less than 200°C), components were calculated for Z57.

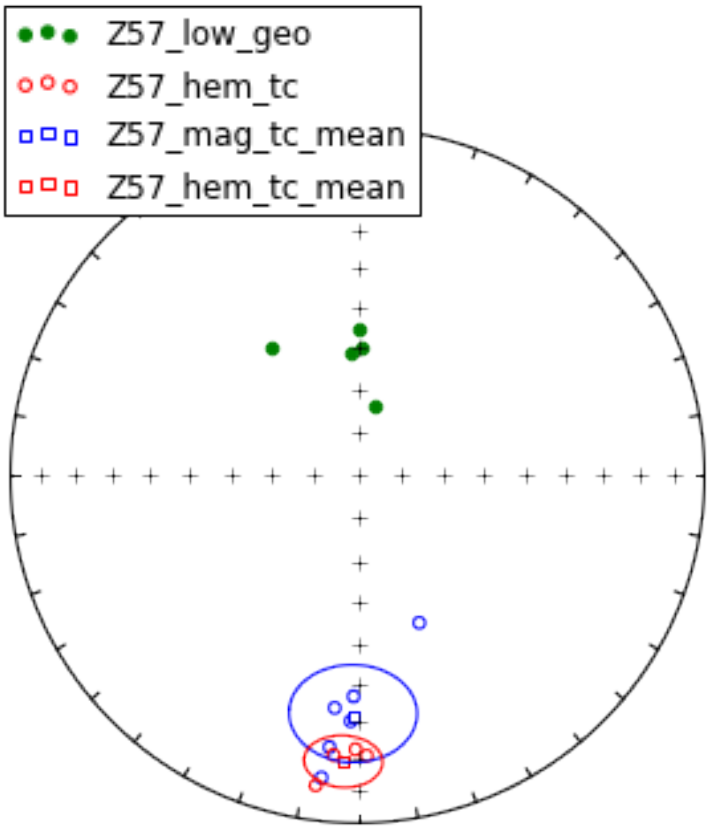

Similar story to flow Z56 - with stark similarities between the magnetite and hematite components.

Z58 Magnetite, mid-, and low- temperature, LOW (less than 200°C), components were calculated for Z58. The middle temperature component derives from demagnetization steps between LOW and magnetite.

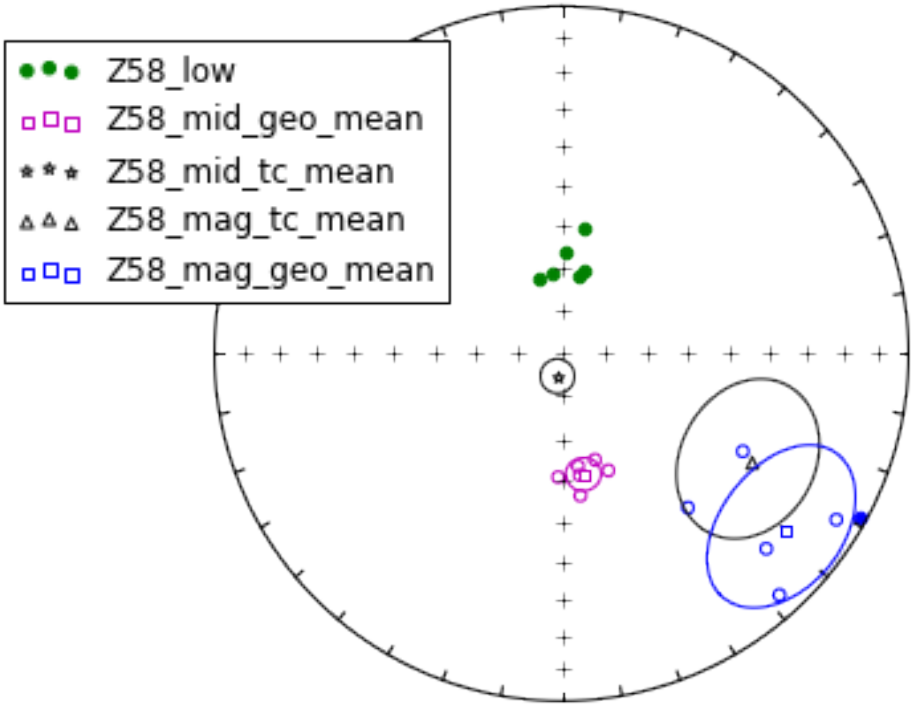

Results from flow Z58 are very different from all of the other sites.

1.1.4 Paleomagnetic data summary

Create tables, distinguished by component type, of mean directions for all Teel flows.

Magnetitie directions

Geographic coordinates - magnetite

Out[67]:

	strat_pos	site_lat	site_lon	dec_geo	inc_geo	alpha95	\
Z30_mag_geo	4	47.10038	95.37550	61.199035	-73.861110	11.712582	
Z31_mag_geo	5	47.10049	95.37604	168.103623	-72.234668	3.753459	
Z32_mag_geo	6	47.10094	95.37684	170.358827	-65.228366	7.987595	

Z33_mag_geo	7	47.10107	95.37705	184.611118	-78.580341	4.579774
Z34_mag_geo	8	47.10111	95.37712	165.710954	-76.241270	2.846954
Z35_mag_geo	9	47.10069	95.37747	180.035625	-56.117492	6.392221
Z36_mag_geo	11	47.10221	95.37959	184.602274	-73.483650	4.160116
Z37_mag_geo	12	47.10211	95.37971	172.808147	-74.694707	7.476051
Z38_mag_geo	13	47.09855	95.38445	170.143849	-68.504682	8.040139
Z39_mag_geo	14	47.09860	95.38467	196.103583	-56.022026	6.360400
Z40_mag_geo	15	47.09859	95.38474	171.882175	-71.414505	4.837145
Z41_mag_geo	10	47.10109	95.37744	175.528998	-59.942821	4.580179
Z42_mag_geo	16	47.09577	95.38577	196.391432	-44.308602	11.150650
Z43_mag_geo	17	47.09570	95.38638	188.500123	-36.936066	10.749181
Z44_mag_geo	18	47.09571	95.38651	177.320106	25.952966	12.333051
Z45_mag_geo	19	47.09562	95.38676	185.281245	22.577189	8.142853
Z46_mag_geo	20	47.09563	95.38692	209.744992	-58.036511	6.728463
Z47_mag_geo	21	47.09568	95.38727	208.133979	-59.587799	5.606451
Z48_mag_geo	22	47.09570	95.38744	207.921657	-49.345442	6.760918
Z49_mag_geo	23	47.09581	95.38747	213.177701	-57.526629	9.488165
Z50_mag_geo	24	47.09575	95.38781	183.717358	16.532802	3.910452
Z51_mag_geo	25	47.09584	95.38802	206.717692	-54.030732	10.393892
Z52_mag_geo	26	47.09583	95.38815	182.835182	-55.213178	12.719642
Z53_mag_geo	1	47.09442	95.37205	172.278467	-71.983776	3.594132
Z54_mag_geo	2	47.09502	95.37299	170.318109	-69.453189	8.193477
Z55_mag_geo	3	47.09525	95.37351	166.386553	-64.854630	5.625088
Z56_mag_geo	27	47.06403	95.42075	179.680351	-4.756236	5.057226
Z57_mag_geo	28	47.06277	95.42039	178.786826	-8.456342	13.052562
Z58_mag_geo	29	47.06277	95.42045	128.167765	-19.352349	17.533117

	n	k	r	csd	paleolatitude	vgp_lat	\
Z30_mag_geo	7	27.513985	6.781929	15.442168	-59.940264	-28.018244	
Z31_mag_geo	8	218.756351	7.968001	5.476520	-57.348450	-77.463763	
Z32_mag_geo	9	42.504477	8.811785	12.424178	-47.295204	-83.450449	
Z33_mag_geo	8	147.251468	7.952462	6.675060	-68.002034	-68.966892	
Z34_mag_geo	10	288.897760	9.968847	4.765549	-63.908090	-71.445651	
Z35_mag_geo	6	110.823428	5.954883	7.694302	-36.670242	-79.569519	
Z36_mag_geo	8	178.256399	7.960731	6.066839	-59.330031	-77.472930	
Z37_mag_geo	9	48.384817	8.834659	11.644758	-61.306496	-75.207168	
Z38_mag_geo	10	37.061501	9.757160	13.305265	-51.774894	-82.077055	
Z39_mag_geo	6	111.925588	5.955327	7.656324	-36.571555	-74.094885	
Z40_mag_geo	9	114.250096	8.929978	7.578037	-56.078745	-79.716310	
Z41_mag_geo	8	147.225628	7.952454	6.675646	-40.828095	-82.952676	
Z42_mag_geo	8	25.632057	7.726904	15.999017	-26.015899	-65.259739	
Z43_mag_geo	8	27.509935	7.745546	15.443305	-20.601392	-62.620370	
Z44_mag_geo	5	39.443485	4.898589	12.897258	13.677537	-29.179269	
Z45_mag_geo	8	47.231012	7.851792	11.786134	11.744294	-30.970825	
Z46_mag_geo	8	68.732148	7.898155	9.770236	-38.705303	-66.823872	
Z47_mag_geo	8	98.575940	7.928989	8.158298	-40.424813	-68.748397	
Z48_mag_geo	8	68.082983	7.897184	9.816705	-30.209549	-62.672462	
Z49_mag_geo	7	41.429419	6.855175	12.584345	-38.154890	-64.234334	

Z50_mag_geo	8	201.619149	7.965281	5.704520	8.442107	-34.363744
Z51_mag_geo	5	55.146896	4.927466	10.907481	-34.565590	-66.394972
Z52_mag_geo	6	28.697188	5.825767	15.120472	-35.744789	-78.453731
Z53_mag_geo	8	238.494787	7.970649	5.245001	-56.957385	-79.068440
Z54_mag_geo	8	46.660914	7.849982	11.857917	-53.143586	-81.346675
Z55_mag_geo	8	97.930102	7.928520	8.185155	-46.807981	-80.714545
Z56_mag_geo	6	176.489683	5.971670	6.097129	-2.382222	-45.317329
Z57_mag_geo	6	27.299686	5.816848	15.502659	-4.251323	-47.175716
Z58_mag_geo	6	15.552391	5.678506	20.539338	-9.960183	-32.768009

	vgp_lon	vgp_lat_rev	vgp_lon_rev
Z30_mag_geo	245.559596	28.018244	65.559596
Z31_mag_geo	244.552326	77.463763	64.552326
Z32_mag_geo	190.612182	83.450449	10.612182
Z33_mag_geo	280.189909	68.966892	100.189909
Z34_mag_geo	255.430852	71.445651	75.430852
Z35_mag_geo	95.219636	79.569519	275.219636
Z36_mag_geo	286.256471	77.472930	106.256471
Z37_mag_geo	261.763513	75.207168	81.763513
Z38_mag_geo	225.175390	82.077055	45.175390
Z39_mag_geo	41.007252	74.094885	221.007252
Z40_mag_geo	249.190583	79.716310	69.190583
Z41_mag_geo	124.113660	82.952676	304.113660
Z42_mag_geo	58.086778	65.259739	238.086778
Z43_mag_geo	77.877325	62.620370	257.877325
Z44_mag_geo	98.369133	29.179269	278.369133
Z45_mag_geo	89.353703	30.970825	269.353703
Z46_mag_geo	15.721243	66.823872	195.721243
Z47_mag_geo	13.361225	68.748397	193.361225
Z48_mag_geo	33.565359	62.672462	213.565359
Z49_mag_geo	13.523120	64.234334	193.523120
Z50_mag_geo	90.931921	34.363744	270.931921
Z51_mag_geo	27.782142	66.394972	207.782142
Z52_mag_geo	83.817965	78.453731	263.817965
Z53_mag_geo	252.646197	79.068440	72.646197
Z54_mag_geo	233.270089	81.346675	53.270089
Z55_mag_geo	188.596346	80.714545	8.596346
Z56_mag_geo	95.874936	45.317329	275.874936
Z57_mag_geo	97.200362	47.175716	277.200362
Z58_mag_geo	162.478280	32.768009	342.478280

High-temperature magnetite (geographic) directions for Teel basalt flows

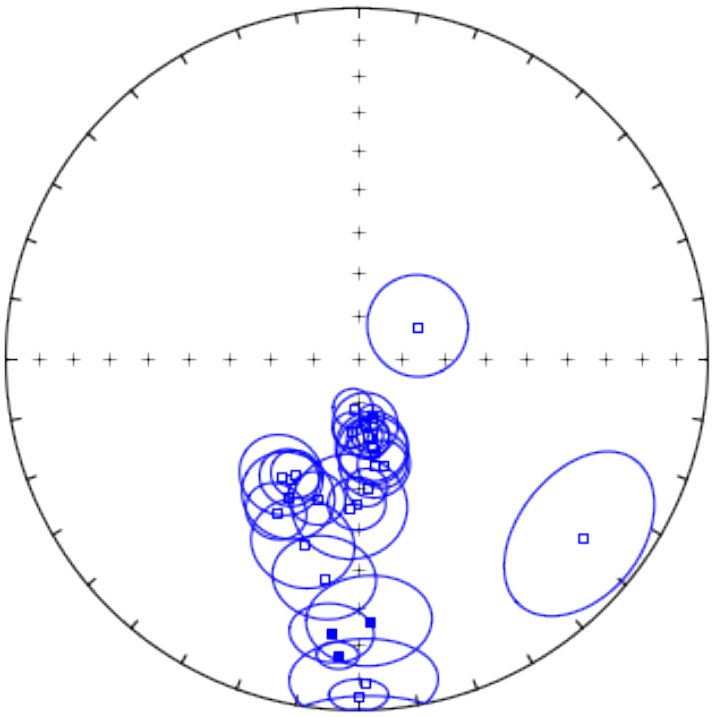

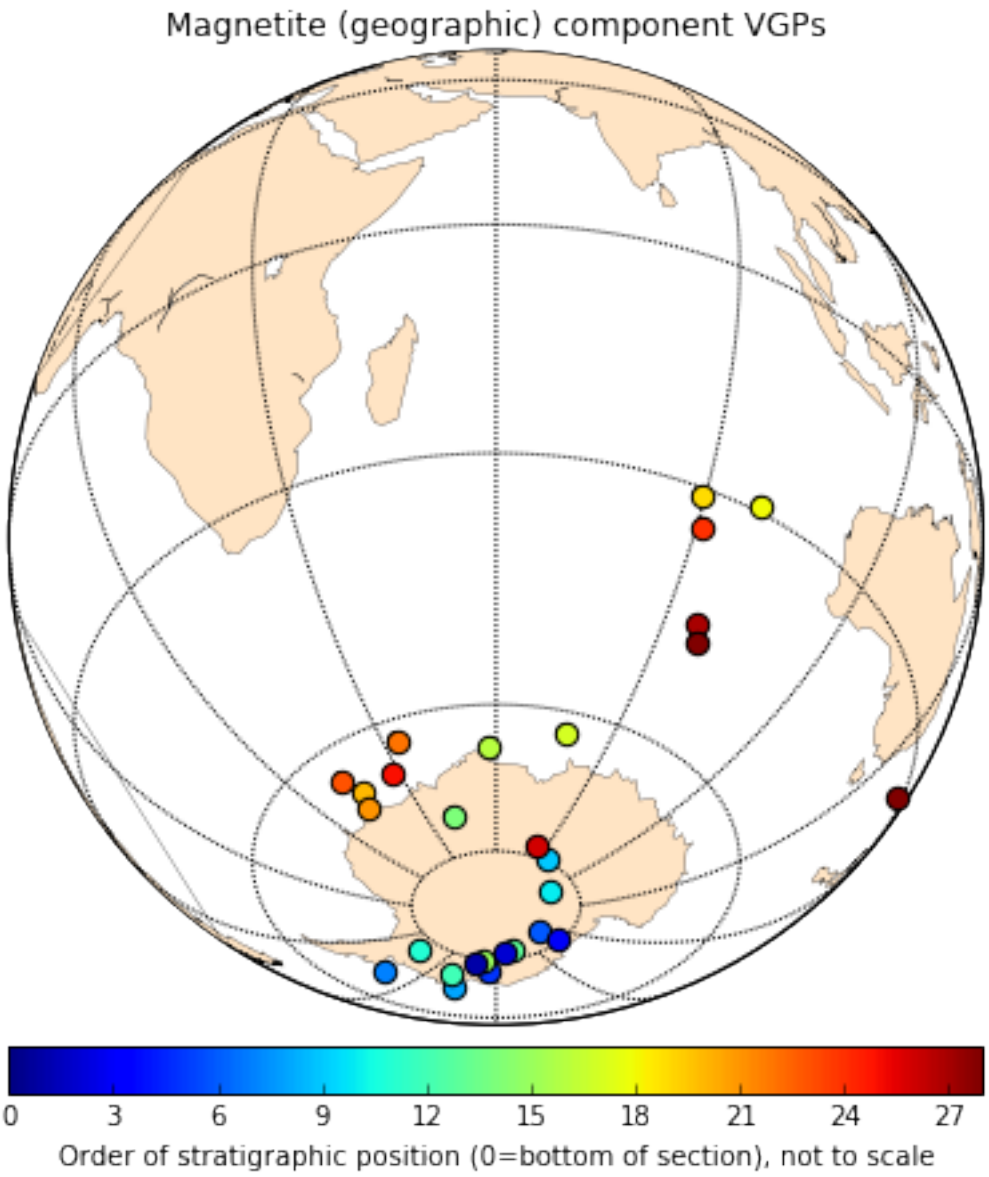

Tilt-corrected coordinates - magnetite

Out[70]:

	strat_pos	site_lat	site_lon	dec_tc	inc_tc	alpha95	n
Z30_mag	4	47.10038	95.37550	278.379367	-46.010280	11.715664	7
Z31_mag	5	47.10049	95.37604	246.928001	-33.319165	3.753646	8
Z32_mag	6	47.10094	95.37684	234.132395	-32.854953	7.997970	9
Z33_mag	7	47.10107	95.37705	250.685156	-32.176114	4.581718	8
Z34_mag	8	47.10111	95.37712	247.131951	-35.840117	2.844796	10
Z35_mag	9	47.10069	95.37747	226.181747	-25.332749	6.399180	6
Z36_mag	11	47.10221	95.37959	247.531592	-39.317142	4.170654	8
Z37_mag	12	47.10211	95.37971	248.052322	-42.739898	7.478423	9

Z38_mag	13	47.09855	95.38445	237.351592	-42.681665	8.027422	10
Z39_mag	14	47.09860	95.38467	230.880551	-26.400672	6.363220	6
Z40_mag	15	47.09859	95.38474	241.380972	-42.753133	4.822532	9
Z41_mag	10	47.10109	95.37744	229.065998	-29.074319	4.590751	8
Z42_mag	16	47.09577	95.38577	219.102263	-24.487183	11.152830	8
Z43_mag	17	47.09570	95.38638	208.946090	-22.598975	10.757156	8
Z44_mag	18	47.09571	95.38651	160.933464	20.616106	12.332689	5
Z45_mag	19	47.09562	95.38676	169.181253	22.723096	8.151115	8
Z46_mag	20	47.09563	95.38692	235.938073	-30.336640	6.723991	8
Z47_mag	21	47.09568	95.38727	236.225390	-32.077321	5.605537	8
Z48_mag	22	47.09570	95.38744	227.700040	-32.087392	6.771057	8
Z49_mag	23	47.09581	95.38747	235.973353	-37.612989	9.479951	7
Z50_mag	24	47.09575	95.38781	175.405740	15.829522	3.922362	8
Z51_mag	25	47.09584	95.38802	229.796663	-36.494284	10.382678	5
Z52_mag	26	47.09583	95.38815	216.149983	-45.789543	12.698064	6
Z53_mag	1	47.09442	95.37205	246.701511	-31.999187	3.599051	8
Z54_mag	2	47.09502	95.37299	243.678159	-32.414475	8.199873	8
Z55_mag	3	47.09525	95.37351	238.040663	-33.518307	5.611932	8
Z56_mag	27	47.06403	95.42075	181.601802	-27.881082	5.069905	6
Z57_mag	28	47.06277	95.42039	181.062329	-31.634060	13.082813	6
Z58_mag	29	47.06277	95.42045	119.444412	-37.602921	17.552705	6

	k	r	csd	paleolatitude	vgp_lat	\
Z30_mag	27.500012	6.781818	15.446091	-27.381947	-14.408220	
Z31_mag	218.734693	7.967998	5.476791	-18.194560	-28.826591	
Z32_mag	42.396758	8.811306	12.439952	-17.895640	-37.203135	
Z33_mag	147.127336	7.952422	6.677876	-17.462312	-25.759713	
Z34_mag	289.334789	9.968894	4.761948	-19.856873	-29.843343	
Z35_mag	110.584559	5.954786	7.702608	-13.316749	-38.856026	
Z36_mag	177.361534	7.960533	6.082124	-22.268860	-31.221631	
Z37_mag	48.354733	8.834556	11.648380	-24.798438	-32.562210	
Z38_mag	37.175977	9.757908	13.284763	-24.753981	-39.808772	
Z39_mag	111.827254	5.955288	7.659690	-13.939647	-36.393048	
Z40_mag	114.937717	8.930397	7.555335	-24.808549	-37.108819	
Z41_mag	146.552710	7.952236	6.690955	-15.536089	-38.748850	
Z42_mag	25.622407	7.726802	16.002029	-12.829071	-42.668310	
Z43_mag	27.470571	7.745182	15.454365	-11.756542	-47.094786	
Z44_mag	39.445745	4.898595	12.896888	10.652755	-29.797321	
Z45_mag	47.137245	7.851497	11.797851	11.826377	-30.288956	
Z46_mag	68.822329	7.898289	9.763833	-16.309766	-34.865831	
Z47_mag	98.607774	7.929012	8.156981	-17.399618	-35.463534	
Z48_mag	67.882078	7.896880	9.831221	-17.406005	-41.018935	
Z49_mag	41.499592	6.855420	12.573700	-21.068304	-38.228444	
Z50_mag	200.402350	7.965070	5.721812	8.068715	-34.684493	
Z51_mag	55.264038	4.927620	10.895915	-20.299603	-41.779935	
Z52_mag	28.791577	5.826338	15.095667	-27.201966	-55.462438	
Z53_mag	237.845848	7.970569	5.252151	-17.350100	-28.388510	
Z54_mag	46.589636	7.849752	11.866984	-17.613960	-30.621692	

Z55_mag	98.385329	7.928851	8.166197	-18.323455	-34.914855
Z56_mag	175.612751	5.971528	6.112333	-14.816796	-57.725144
Z57_mag	27.177964	5.816027	15.537336	-17.119456	-60.043844
Z58_mag	15.519815	5.677831	20.560882	-21.061319	-35.140582

	vgp_lon	vgp_lat_rev	vgp_lon_rev
Z30_mag	340.470733	14.408220	160.470733
Z31_mag	9.314505	28.826591	189.314505
Z32_mag	19.865666	37.203135	199.865666
Z33_mag	7.086542	25.759713	187.086542
Z34_mag	7.791244	29.843343	187.791244
Z35_mag	31.001433	38.856026	211.001433
Z36_mag	5.455763	31.221631	185.455763
Z37_mag	2.867308	32.562210	182.867308
Z38_mag	10.899760	39.808772	190.899760
Z39_mag	26.087975	36.393048	206.087975
Z40_mag	7.746124	37.108819	187.746124
Z41_mag	26.425574	38.748850	206.425574
Z42_mag	38.628730	42.668310	218.628730
Z43_mag	51.278792	47.094786	231.278792
Z44_mag	117.098874	29.797321	297.098874
Z45_mag	107.671016	30.288956	287.671016
Z46_mag	19.680166	34.865831	199.680166
Z47_mag	18.516120	35.463534	198.516120
Z48_mag	26.092301	41.018935	206.092301
Z49_mag	15.487683	38.228444	195.487683
Z50_mag	100.922274	34.684493	280.922274
Z51_mag	21.526652	41.779935	201.526652
Z52_mag	27.657758	55.462438	207.657758
Z53_mag	10.165158	28.388510	190.165158
Z54_mag	12.284724	30.621692	192.284724
Z55_mag	16.200615	34.914855	196.200615
Z56_mag	92.519901	57.725144	272.519901
Z57_mag	93.386864	60.043844	273.386864
Z58_mag	179.028128	35.140582	359.028128

High-temperature magnetite (tilt-corrected) directions for Teel basalt flows

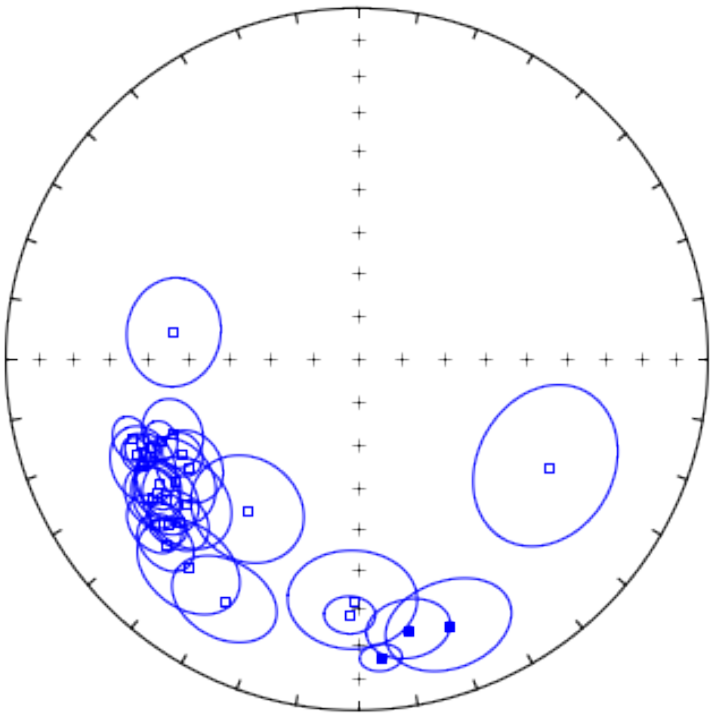

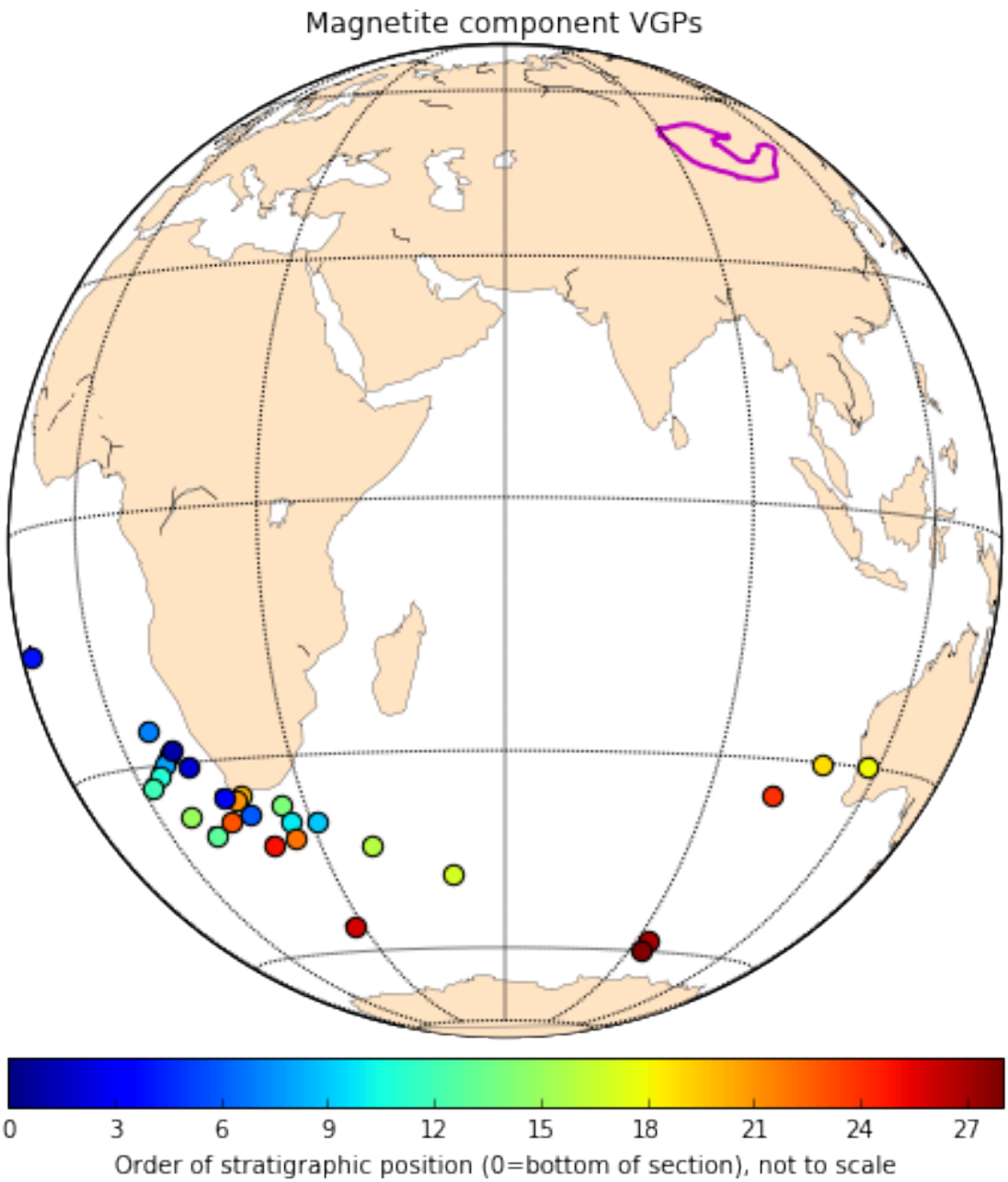

Hematite directions

Geographic coordinates - hematite

Out[73]:

	strat_pos	site_lat	site_lon	dec_geo	inc_geo	alpha95
Z35_hem_geo	4	47.10038	95.37550	185.352162	-5.560896	5.747798
Z30_hem_geo	9	47.10069	95.37747	148.799913	-68.209834	49.957167
Z38_hem_geo	13	47.09855	95.38445	195.565071	-26.364592	8.833229

Z39_hem_geo	14	47.09860	95.38467	196.313095	-15.623428	8.663295
Z40_hem_geo	15	47.09859	95.38474	189.173033	-23.507115	7.794855
Z41_hem_geo	10	47.10109	95.37744	178.834997	-26.225350	16.086290
Z42_hem_geo	16	47.09577	95.38577	165.448451	27.278167	16.388007
Z43_hem_geo	17	47.09570	95.38638	182.753379	12.734651	6.220142
Z44_hem_geo	18	47.09571	95.38651	182.138846	26.690156	2.023836
Z45_hem_geo	19	47.09562	95.38676	179.431606	23.111384	4.657126
Z46_hem_geo	20	47.09563	95.38692	199.630710	23.039855	43.076043
Z47_hem_geo	21	47.09568	95.38727	186.530284	-3.818259	14.407211
Z48_hem_geo	22	47.09570	95.38744	186.680865	20.745840	5.248580
Z49_hem_geo	23	47.09581	95.38747	201.506939	6.066986	11.535574
Z50_hem_geo	24	47.09575	95.38781	185.576900	22.848691	3.695319
Z51_hem_geo	25	47.09584	95.38802	184.630448	22.563173	10.926624
Z52_hem_geo	26	47.09583	95.38815	182.777548	21.100104	13.120981
Z53_hem_geo	1	47.09442	95.37205	176.883446	-21.454440	5.750351
Z54_hem_geo	2	47.09502	95.37299	166.032855	-40.835976	52.801938
Z56_hem_geo	27	47.06403	95.42075	179.194265	1.511589	8.593573
Z57_hem_geo	28	47.06277	95.42039	181.947932	4.332196	7.473594

	n	k	r	csd	paleolatitude	vgp_lat	\
Z35_hem_geo	6	136.842402	5.963462	6.924281	-2.787011	-45.444034	
Z30_hem_geo	7	2.413452	4.513935	52.139357	-51.356099	-69.351223	
Z38_hem_geo	2	801.477440	1.998752	2.861142	-13.918471	-54.362780	
Z39_hem_geo	5	78.962990	4.949343	9.115347	-7.959659	-48.458523	
Z40_hem_geo	7	60.926778	6.901521	10.377217	-12.269627	-54.326542	
Z41_hem_geo	5	23.576274	4.830338	16.681974	-13.836835	-56.721476	
Z42_hem_geo	6	17.664613	5.716948	19.272274	14.457588	-27.077402	
Z43_hem_geo	8	80.262873	7.912787	9.041233	6.446942	-36.401745	
Z44_hem_geo	7	890.663468	6.993263	2.714115	14.109891	-28.764330	
Z45_hem_geo	8	142.431974	7.950854	6.787053	12.045434	-30.856760	
Z46_hem_geo	2	35.743651	1.972023	13.548324	12.005012	-28.348190	
Z47_hem_geo	7	18.506577	6.675791	18.828771	-1.911251	-44.460110	
Z48_hem_geo	8	112.342494	7.937691	7.642105	10.724316	-31.873027	
Z49_hem_geo	6	34.686217	5.855851	13.753288	3.042020	-36.413576	
Z50_hem_geo	8	225.663876	7.968980	5.392051	11.897134	-30.796567	
Z51_hem_geo	5	49.990867	4.919985	11.456176	11.736415	-31.022182	
Z52_hem_geo	6	27.025581	5.814990	15.581078	10.920183	-31.930956	
Z53_hem_geo	7	111.157505	6.946023	7.682731	-11.116766	-53.926099	
Z54_hem_geo	8	2.056913	4.596843	56.477701	-23.370939	-63.768703	
Z56_hem_geo	6	61.741195	5.919017	10.308548	0.755926	-42.174837	
Z57_hem_geo	4	152.109621	3.980277	6.567600	2.169198	-40.738280	

	vgp_lon	vgp_lat_rev	vgp_lon_rev
Z35_hem_geo	87.744611	45.444034	267.744611
Z30_hem_geo	208.833918	69.351223	28.833918
Z38_hem_geo	68.832083	54.362780	248.832083
Z39_hem_geo	70.583219	48.458523	250.583219
Z40_hem_geo	79.891757	54.326542	259.891757

Z41_hem_geo	97.439300	56.721476	277.439300
Z42_hem_geo	111.243174	27.077402	291.243174
Z43_hem_geo	91.986451	36.401745	271.986451
Z44_hem_geo	93.020083	28.764330	273.020083
Z45_hem_geo	96.034300	30.856760	276.034300
Z46_hem_geo	73.462329	28.348190	253.462329
Z47_hem_geo	86.223719	44.460110	266.223719
Z48_hem_geo	87.651814	31.873027	267.651814
Z49_hem_geo	68.327763	36.413576	248.327763
Z50_hem_geo	89.031882	30.796567	269.031882
Z51_hem_geo	90.095926	31.022182	270.095926
Z52_hem_geo	92.174224	31.930956	272.174224
Z53_hem_geo	100.570110	53.926099	280.570110
Z54_hem_geo	125.457583	63.768703	305.457583
Z56_hem_geo	96.507901	42.174837	276.507901
Z57_hem_geo	92.851012	40.738280	272.851012

Hematite directions from Teel basalt flows in geographic coordinates

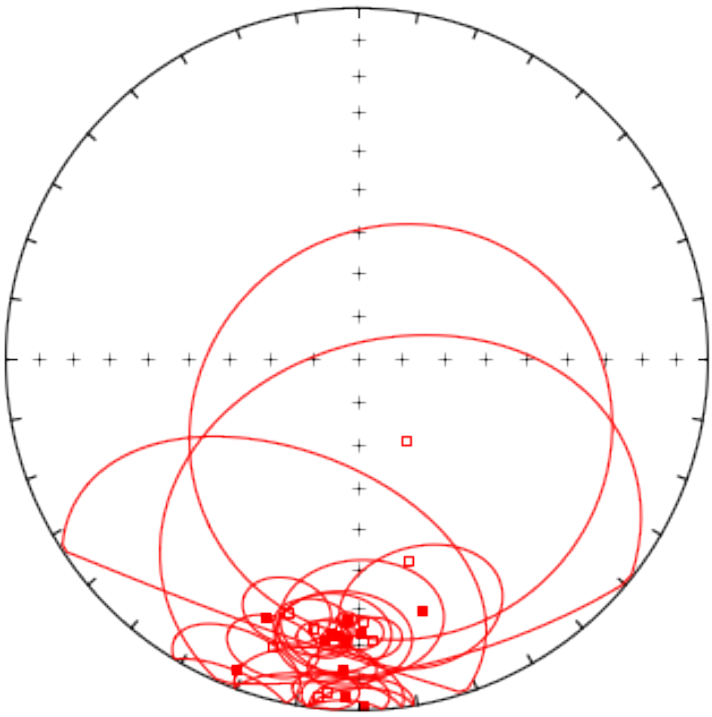

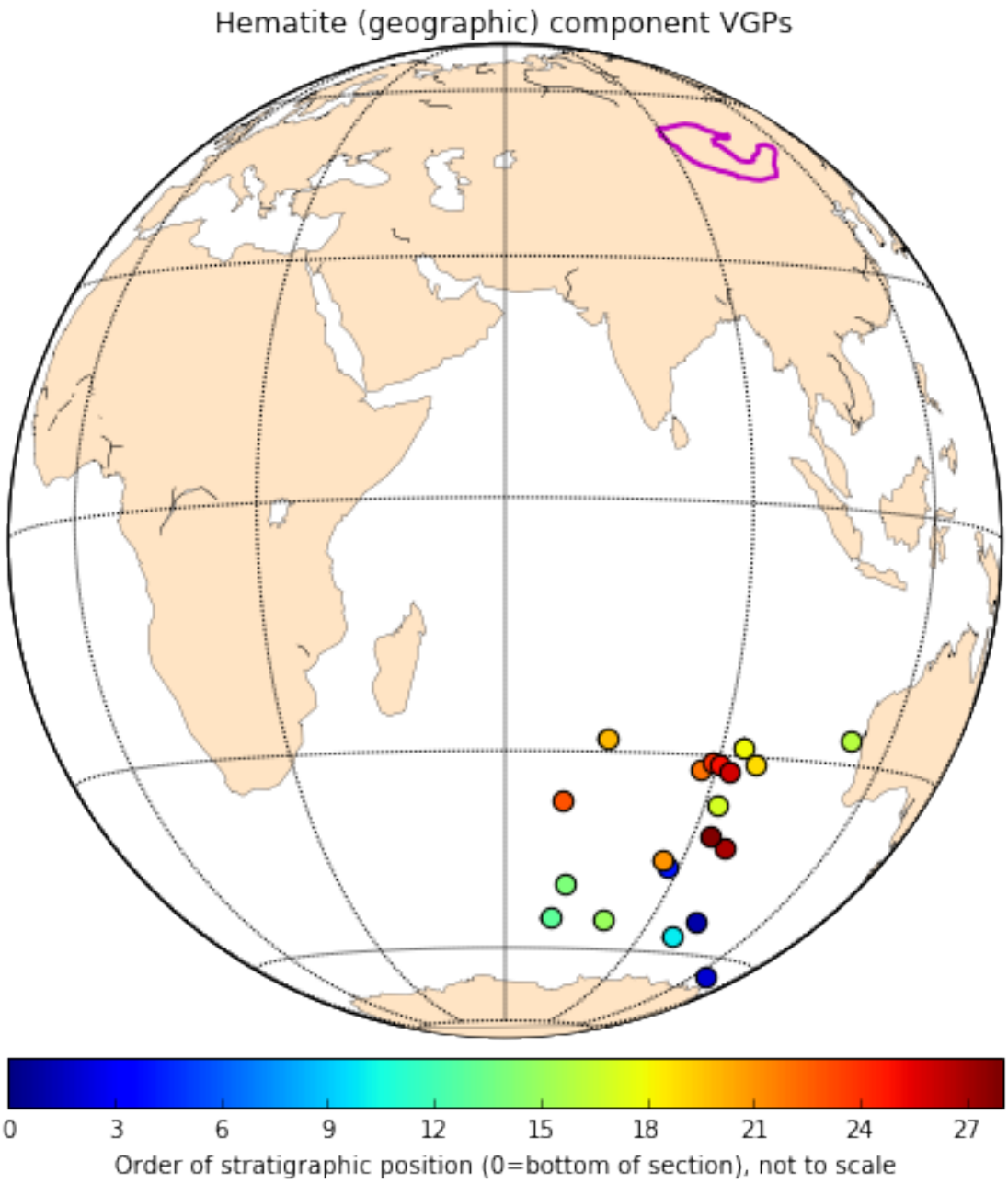

Tilt-corrected coordinates - hematite

Out[76]:

	strat_pos	site_lat	site_lon	dec_tc	inc_tc	alpha95	n	\
Z35_hem	4	47.10038	95.37550	185.114311	6.025809	5.727598	6	
Z30_hem	9	47.10069	95.37747	242.928054	-40.237690	49.931876	7	
Z38_hem	13	47.09855	95.38445	208.352571	-5.900502	8.908547	2	
Z39_hem	14	47.09860	95.38467	201.539571	2.413034	8.658960	5	
Z40_hem	15	47.09859	95.38474	202.157748	-7.928196	7.788149	7	

Z41_hem	10	47.10109	95.37744	198.411151	-11.058439	16.113432	5
Z42_hem	16	47.09577	95.38577	151.386122	14.995751	16.374487	6
Z43_hem	17	47.09570	95.38638	173.787706	13.587096	6.227989	8
Z44_hem	18	47.09571	95.38651	163.946455	23.981346	2.033549	7
Z45_hem	19	47.09562	95.38676	164.416633	19.689336	4.665334	8
Z46_hem	20	47.09563	95.38692	180.134056	31.708243	43.051197	2
Z47_hem	21	47.09568	95.38727	186.913270	2.679432	14.418197	7
Z48_hem	22	47.09570	95.38744	175.819816	20.880528	5.256939	8
Z49_hem	23	47.09581	95.38747	196.482372	14.863765	11.529913	6
Z50_hem	24	47.09575	95.38781	173.713227	22.176830	3.699165	8
Z51_hem	25	47.09584	95.38802	173.080330	21.478208	10.923883	5
Z52_hem	26	47.09583	95.38815	172.236460	19.385124	13.100041	6
Z53_hem	1	47.09442	95.37205	195.874742	-12.092261	5.754882	7
Z54_hem	2	47.09502	95.37299	210.517882	-28.621488	52.793211	8
Z56_hem	27	47.06403	95.42075	180.301491	-21.711722	8.592210	6
Z57_hem	28	47.06277	95.42039	182.841002	-18.592084	7.462069	4

	k	r	csd	paleolatitude	vgp_lat	\
Z35_hem	137.802632	5.963716	6.900114	3.021259	-39.676603	
Z30_hem	2.414928	4.515454	52.123423	-22.933069	-34.802858	
Z38_hem	788.017587	1.998731	2.885473	-2.958094	-39.500385	
Z39_hem	79.041121	4.949393	9.110841	1.207052	-38.143076	
Z40_hem	61.030111	6.901688	10.368429	-3.983165	-42.830083	
Z41_hem	23.500114	4.829788	16.708984	-5.581195	-45.565273	
Z42_hem	17.692229	5.717390	19.257227	7.628503	-29.676516	
Z43_hem	80.063147	7.912569	9.052503	6.890414	-35.733259	
Z44_hem	882.184819	6.993199	2.727126	12.539568	-28.658505	
Z45_hem	141.934618	7.950682	6.798934	10.144077	-31.097230	
Z46_hem	35.782409	1.972053	13.540984	17.166216	-25.738041	
Z47_hem	18.479833	6.675322	18.842390	1.340449	-41.186055	
Z48_hem	111.988554	7.937494	7.654172	10.798704	-31.985346	
Z49_hem	34.719353	5.855988	13.746724	7.559053	-33.419750	
Z50_hem	225.196841	7.968916	5.397639	11.519700	-31.115698	
Z51_hem	50.015473	4.920025	11.453358	11.129977	-31.446845	
Z52_hem	27.109018	5.815560	15.557081	9.978044	-32.507612	
Z53_hem	110.984038	6.945938	7.688733	-6.114213	-46.812655	
Z54_hem	2.057276	4.597443	56.472722	-15.261779	-49.341300	
Z56_hem	61.760484	5.919042	10.306938	-11.259937	-54.195001	
Z57_hem	152.576865	3.980338	6.557536	-9.547317	-52.406934	

	vgp_lon	vgp_lat_rev	vgp_lon_rev
Z35_hem	88.733786	39.676603	268.733786
Z30_hem	8.295178	34.802858	188.295178
Z38_hem	57.459211	39.500385	237.459211
Z39_hem	67.563030	38.143076	247.563030
Z40_hem	64.518459	42.830083	244.518459
Z41_hem	68.698517	45.565273	248.698517
Z42_hem	128.501026	29.676516	308.501026

Z43_hem	102.991555	35.733259	282.991555
Z44_hem	113.302682	28.658505	293.302682
Z45_hem	113.374942	31.097230	293.374942
Z46_hem	95.244729	25.738041	275.244729
Z47_hem	86.186406	41.186055	266.186406
Z48_hem	100.230031	31.985346	280.230031
Z49_hem	75.695091	33.419750	255.695091
Z50_hem	102.587676	31.115698	282.587676
Z51_hem	103.352735	31.446845	283.352735
Z52_hem	104.465028	32.507612	284.465028
Z53_hem	71.955927	46.812655	251.955927
Z54_hem	46.618190	49.341300	226.618190
Z56_hem	94.915322	54.195001	274.915322
Z57_hem	90.824846	52.406934	270.824846

Hematite (tilt-corrected) directions from Teel basalt flows

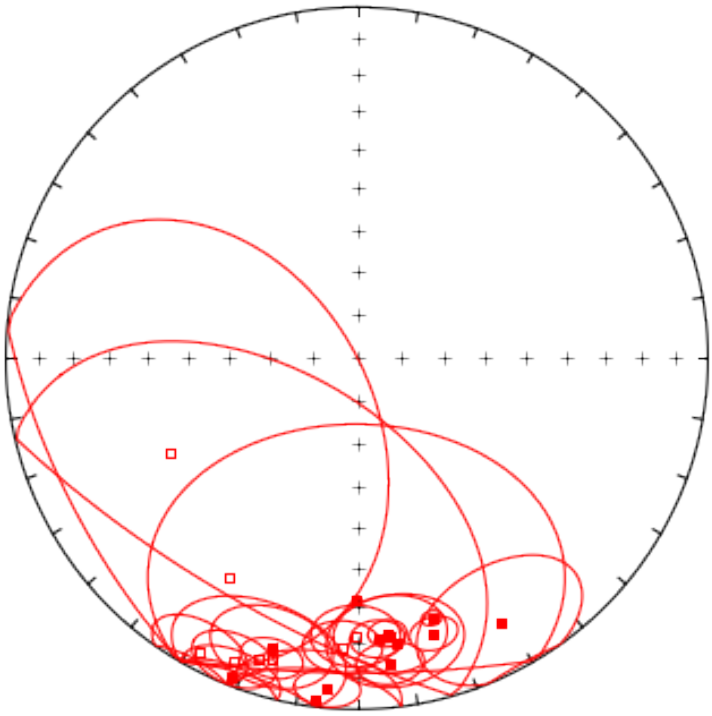

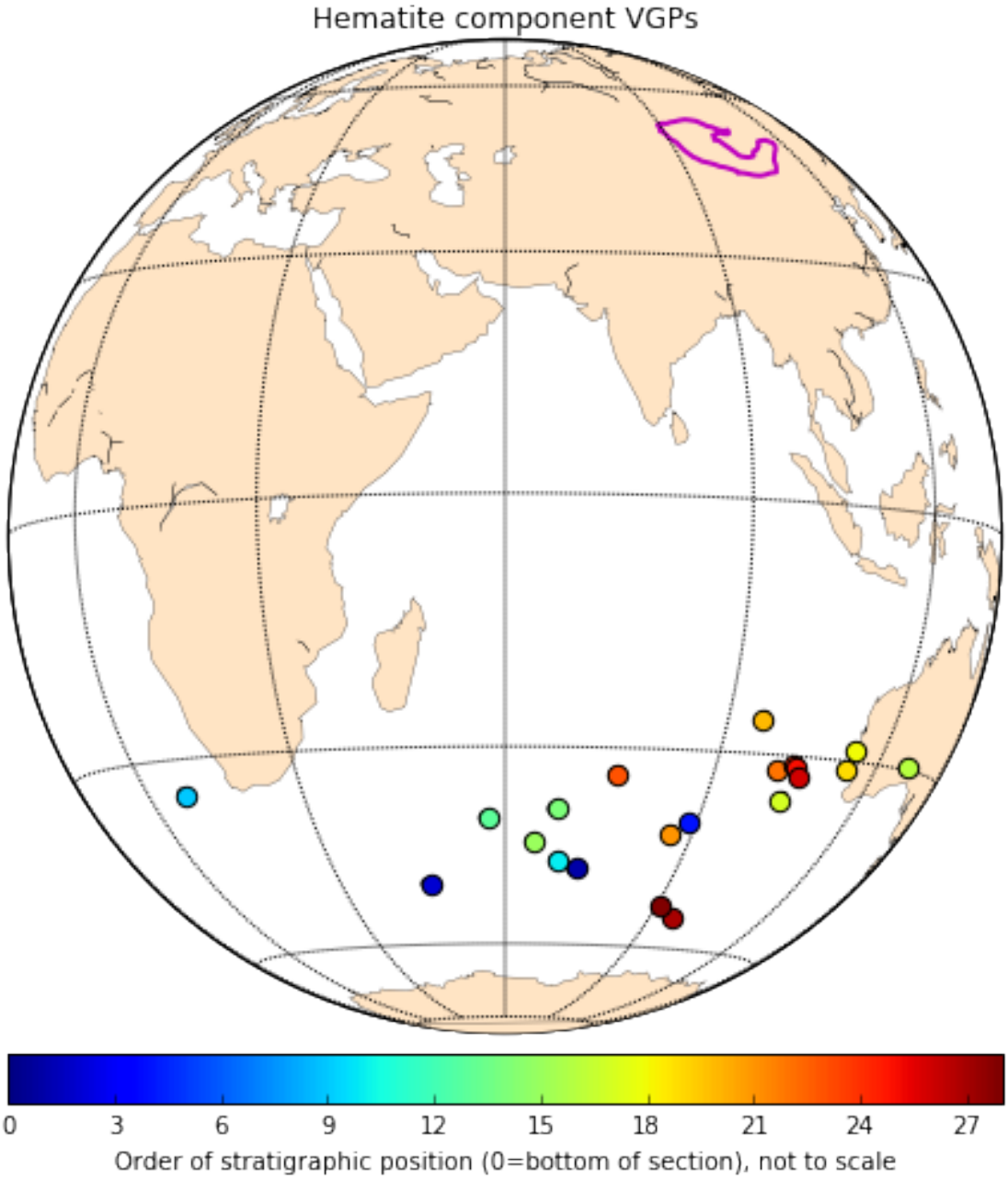

Mid-temperature directions

Out[79]:

	strat_pos	site_lat	site_lon	dec_geo	inc_geo	alpha95	n	\
Z42_mid	16	47.09577	95.38577	332.936127	-68.973663	22.704625	4	
Z43_mid	17	47.09570	95.38638	214.749151	-62.316153	27.256978	4	
Z58_mid	29	47.06277	95.42045	169.686782	-61.093602	4.004771	6	

	k	r	csd	paleolatitude	vgp_lat	\
Z42_mid	17.342624	3.827016	19.450359	-52.447527	-12.194273	
Z43_mid	12.329873	3.756688	23.067776	-43.621783	-65.542782	
Z58_mid	280.878503	5.982199	4.833100	-42.161138	-81.183719	

	vgp_lon	vgp_lat_rev	vgp_lon_rev
Z42_mid	291.867415	12.194273	111.867415
Z43_mid	0.679322	65.542782	180.679322
Z58_mid	155.401297	81.183719	335.401297

Mid-temperature directions from Teel basalt flows in geographic coordinates

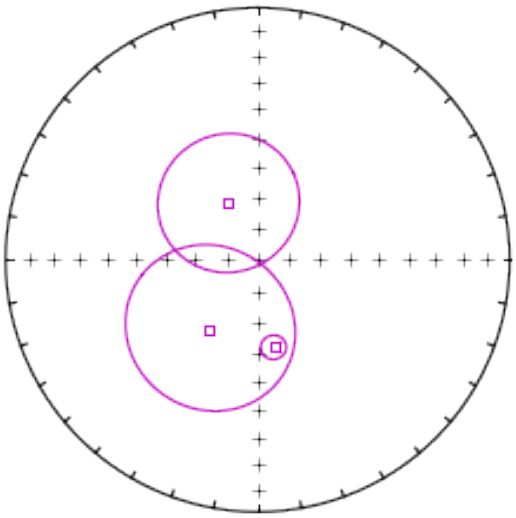

Flow Z58 yielded a completely different mid-temperature result compared to all other sites. The magnetite direction is completely different than all other results. The mean direction is very imprecise (SE and moderately-shallow down) but is closest in orientation to the Middle to Late Carboniferous 'A' component of Edel et al. (2014).

1.1.5 Paleomagnetic Poles for the Teel Formation

We beleive that the primary paleomagnetic pole for the Teel basalts is held by magnetite in some form (i.e., magnetite with slightly different amounts of titanium). However, demagnetization data from some sites show similarities to the remanence directions of magnetite and hematite. We suspect that the hematite directions were acquired later in the Paleozoic Era, therefore when

the magnetite remanence is similar to that of hematite we suspect that the magnetite has been chemically overprinted by dominant amounts of hematite.

Primary magnetite pole - including fold test All of these mean directions are derived from unblocking temperatures in the magnetite range. However, we beleive that a number of sites yield samples where the hematite remanence demagnetizes at the same time as magnetite, therefore preventing a measurement of the pure magnetite magnetization. When this behavior is suspected or evident in samples or sites, those results are documented and excluded.

```
Out[83]: {'alpha95': 4.9431252055096131,
          'csd': 13.058928417331206,
          'dec': 236.6128693429381,
          'inc': -34.995940978983391,
          'k': 38.472902790170508,
          'n': 23,
          'r': 22.428168960372265}

Out[84]: {'alpha95': 5.7116821039230583,
          'csd': 15.025346173655382,
          'dec': 186.62753154703333,
          'inc': -64.852074989296611,
          'k': 29.061703291478157,
          'n': 23,
          'r': 22.24299000029874}
```

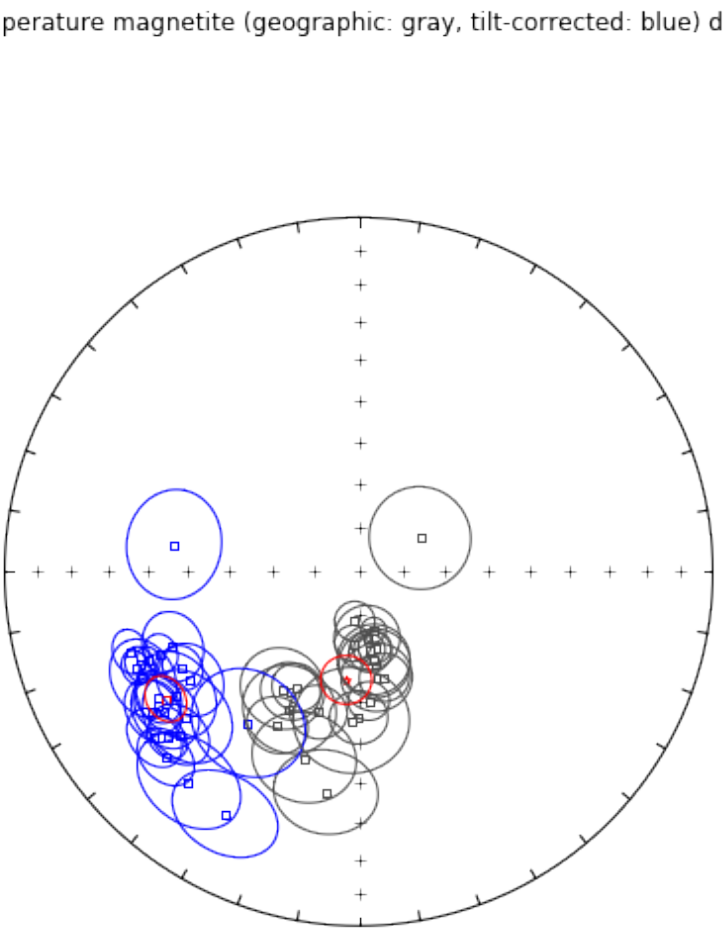

Bootstrap fold test (Tauxe and Watson, 1994)

```
doing  1000  iterations...please be patient...
```

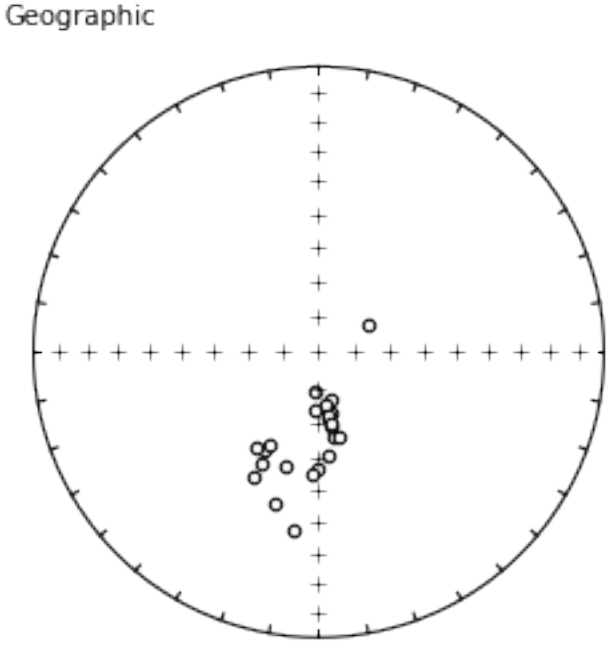
Geographic

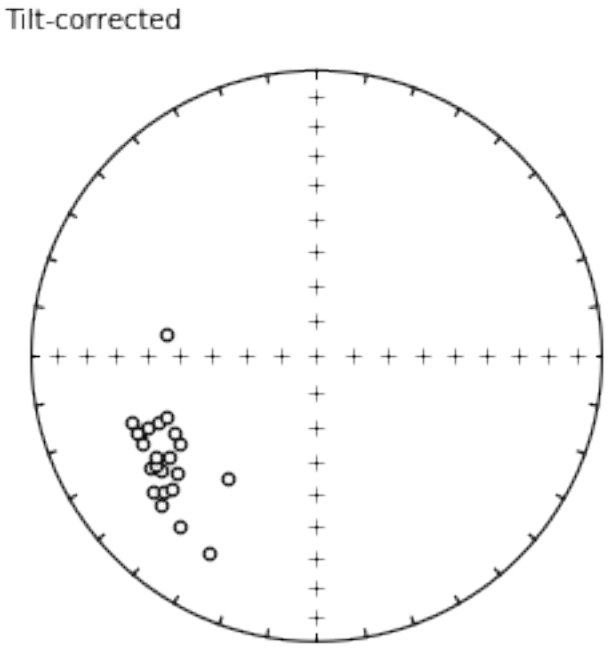

tightest grouping of vectors obtained at (95% confidence bounds):
52 - 97 percent unfolding
range of all bootstrap samples:
37 - 109 percent unfolding

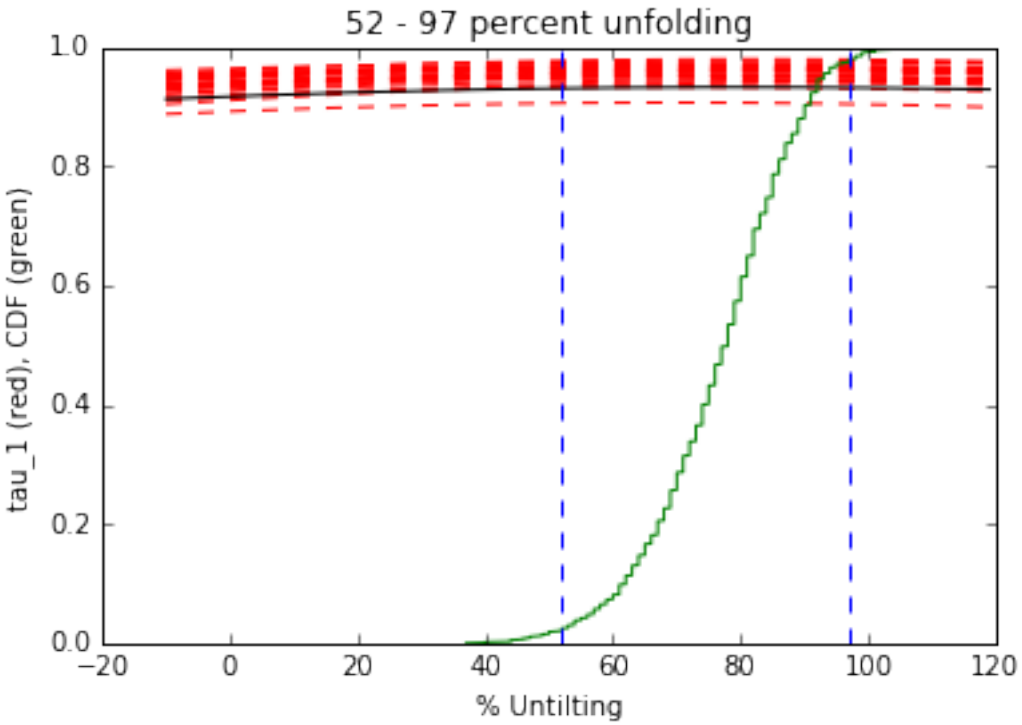

Below the tilt-corrected magnetite VGPs are plotted on the globe and shaded according to their relative stratigraphic positions.

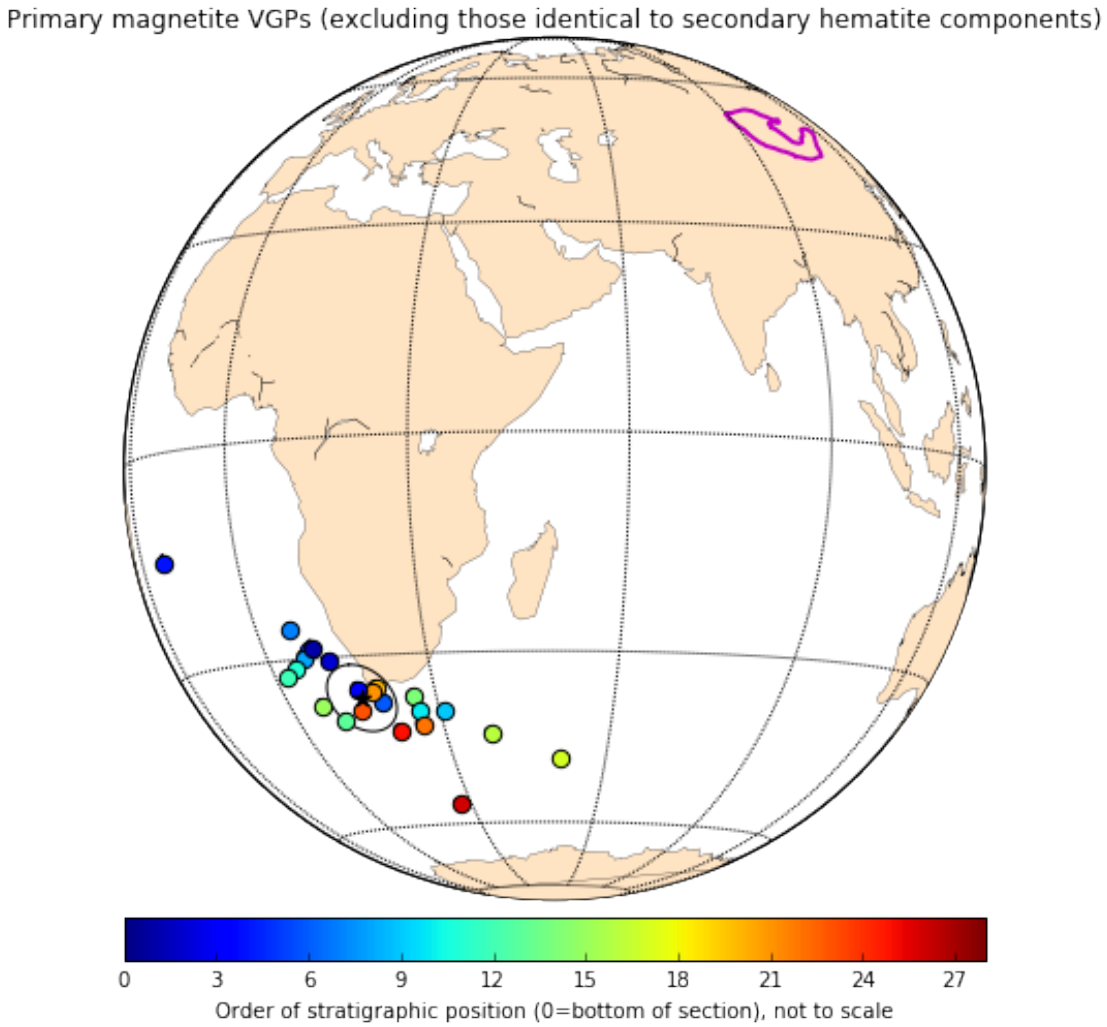

Secondary hematite pole - including fold test

```
Out[90]: {'alpha95': 9.2608689622177227,
          'csd': 20.97901071644646,
          'dec': 184.58560616364625,
          'inc': 3.8459585385145614,
          'k': 14.907335584818336,
          'n': 18,
          'r': 16.85962183494998}

Out[91]: {'alpha95': 9.4955663885263011,
          'csd': 21.474669531178204,
          'dec': 182.89089648457883,
          'inc': 6.1094491428847837,
          'k': 14.227122114351561,
```

```
'n': 18,
'r': 16.805099171613119}
```

High-temperature hematite (geographic: gray/red, tilt-corrected: yellow/blue) directions

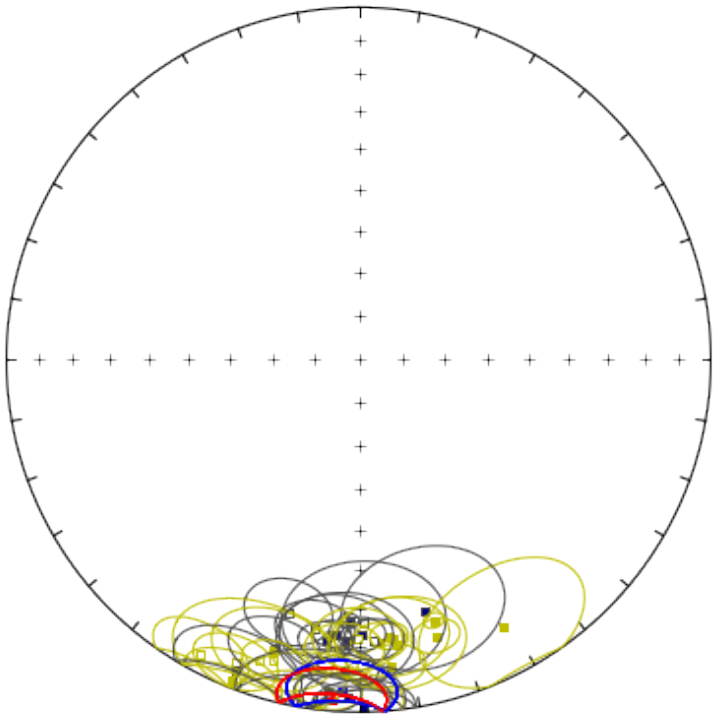

Bootstrap fold test (Tauxe and Watson, 1994)

```
doing  1000  iterations...please be patient...
```

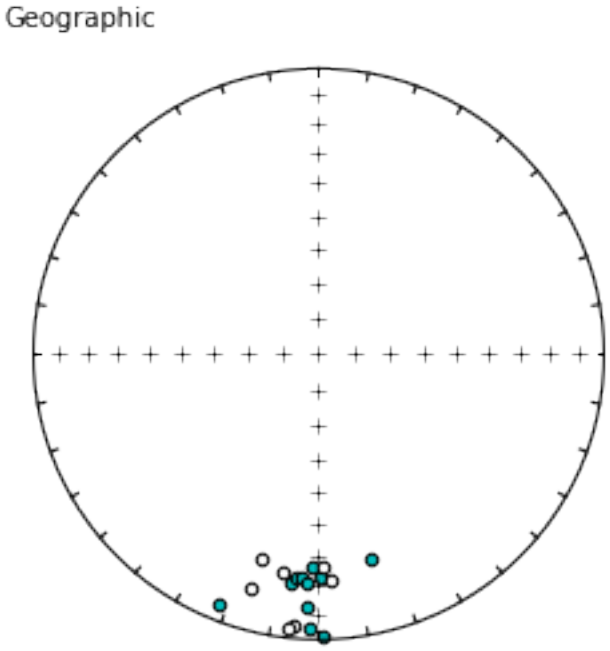
Geographic

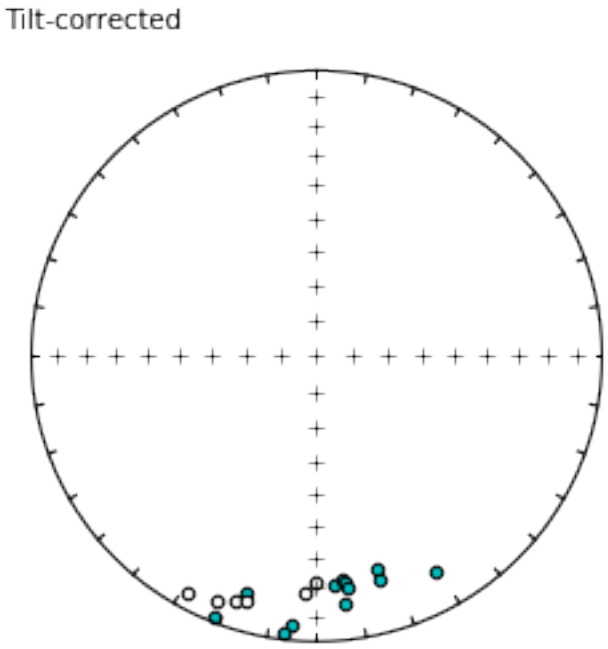


```
tightest grouping of vectors obtained at (95% confidence bounds):
-20 - 119 percent unfolding
range of all bootstrap samples:
-20  -  119 percent unfolding
```

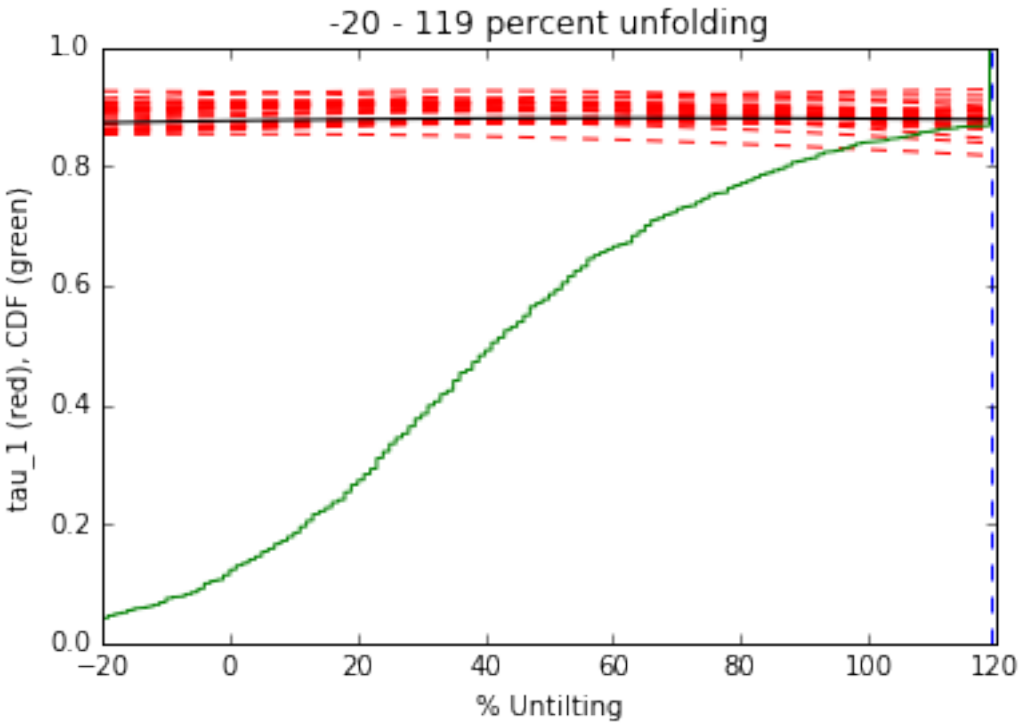

Below the geographic and tilt-corrected hematite VGPs are plotted on the globe and shaded according to their relative stratigraphic positions. Note the similar positions between the two coordinate system means.

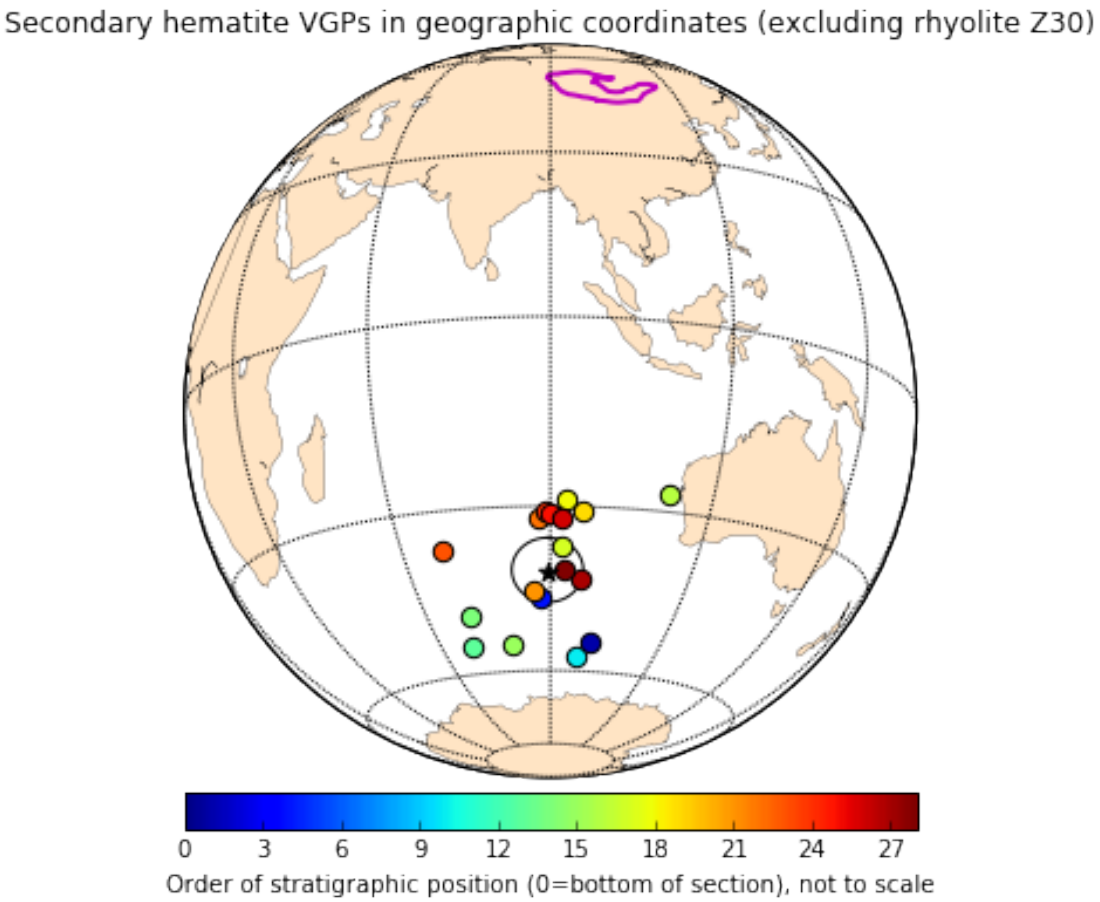
Secondary hematite VGPs in geographic coordinates (excluding rhyolite Z30)
0
3
6
9
12
15
18
21
24
27
Order of stratigraphic position (0=bottom of section), not to scale

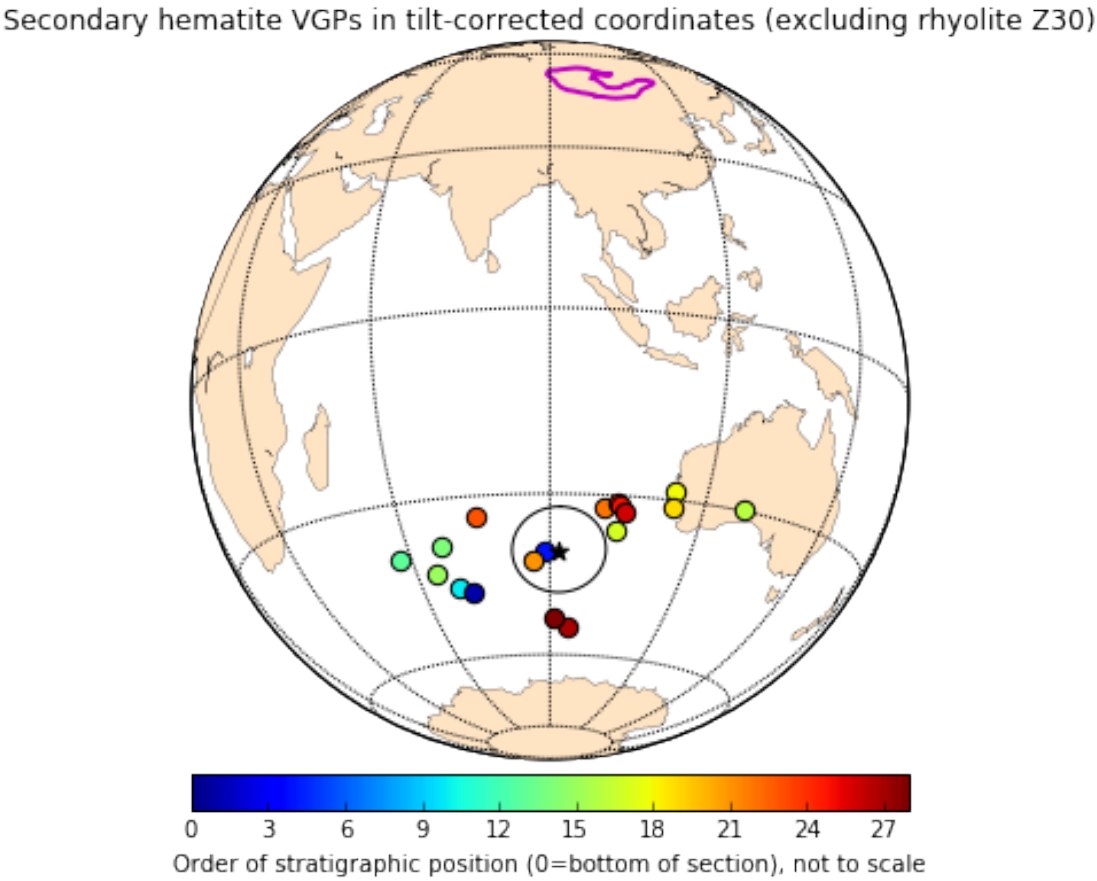

Present local field overprint - negative fold test

Out[96]:

	strat_pos	site_lat	site_lon	dec_geo	inc_geo	alpha95
Z30_low_geo	4	47.10038	95.37550	346.473053	68.261419	11.458361
Z31_low_geo	5	47.10049	95.37604	0.054372	64.923839	3.618073
Z32_low_geo	6	47.10094	95.37684	25.452043	61.325382	8.812910
Z33_low_geo	7	47.10107	95.37705	0.930272	64.380739	6.003504
Z34_low_geo	8	47.10111	95.37712	0.648074	62.405014	3.865736

	n	k	r	csd	paleolatitude	vgp_lat
Z30_low_geo	7	28.705783	6.790983	15.118208	51.429142	80.188638
Z31_low_geo	8	235.361535	7.970259	5.279798	46.897847	89.793993
Z32_low_geo	8	40.461392	7.826996	12.733993	42.434489	71.428192
Z33_low_geo	8	86.089978	7.918690	8.729889	46.196993	88.893147
Z34_low_geo	10	157.128808	9.942722	6.461854	43.729780	86.598151

	vgp_lon	vgp_lat_rev	vgp_lon_rev
Z30_low_geo	36.526238	-80.188638	216.526238
Z31_low_geo	264.986185	-89.793993	84.986185

```
Z32_low_geo  190.579622   -71.428192    10.579622
Z33_low_geo  239.802233   -88.893147    59.802233
Z34_low_geo  267.460060   -86.598151    87.460060
```

Out[97]:

	strat_pos	site_lat	site_lon	dec_tc	inc_tc	alpha95	n
Z30_low	4	47.10038	95.37550	62.140855	33.713657	11.463681	7
Z31_low	5	47.10049	95.37604	59.403835	27.876060	3.615270	8
Z32_low	6	47.10094	95.37684	25.452043	61.325382	8.812910	8
Z33_low	7	47.10107	95.37705	54.800714	28.344304	6.009620	8
Z34_low	8	47.10111	95.37712	52.688703	27.653908	3.866823	10

	k	r	csd	paleolatitude	vgp_lat
Z30_low	28.680029	6.790795	15.124995	18.450285	32.248029
Z31_low	235.725142	7.970304	5.275724	14.813793	31.483537
Z32_low	40.461392	7.826996	12.733993	42.434489	71.428192
Z33_low	85.916769	7.918526	8.738684	15.094685	34.722681
Z34_low	157.041051	9.942690	6.463659	14.681124	35.788473

	vgp_lon	vgp_lat_rev	vgp_lon_rev
Z30_low	192.800152	-32.248029	12.800152
Z31_low	198.002746	-31.483537	18.002746
Z32_low	190.579622	-71.428192	10.579622
Z33_low	201.658195	-34.722681	21.658195
Z34_low	203.849471	-35.788473	23.849471

A number of poles are excluded because of inconsistencies between samples within site which resulted in large a95 values for these sites: Z45, Z51, and Z52.

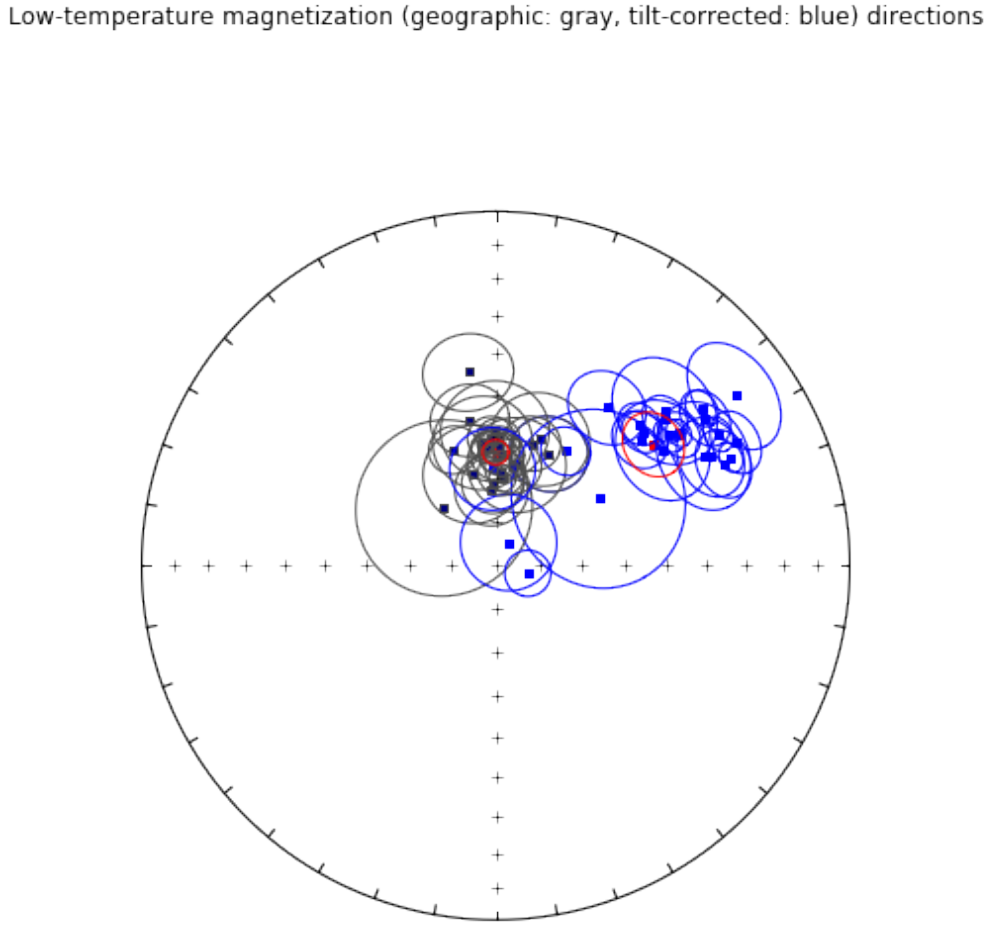

Bootstrap fold test (Tauxe and Watson, 1994)

```
doing  1000  iterations...please be patient...
```

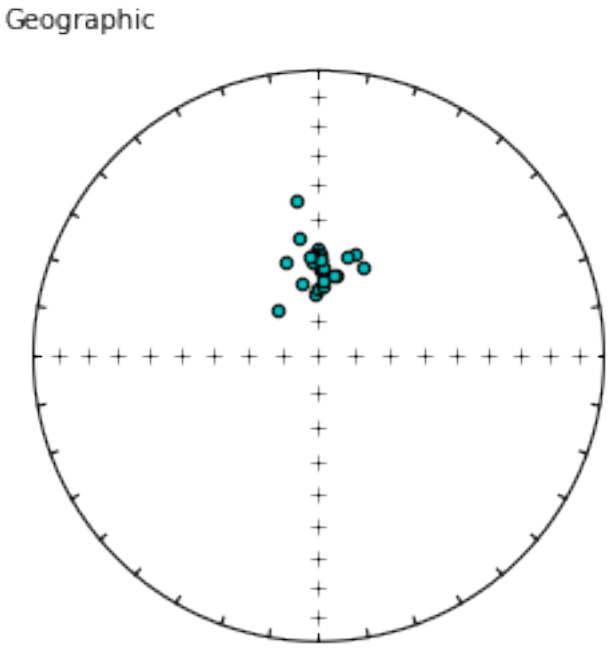
Geographic

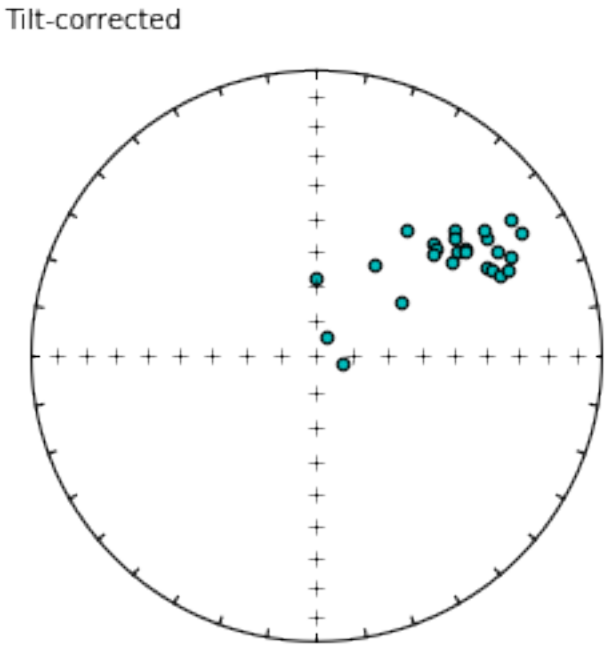


```
tightest grouping of vectors obtained at (95% confidence bounds):
-18 - 10 percent unfolding
range of all bootstrap samples:
-20  -  28 percent unfolding
```

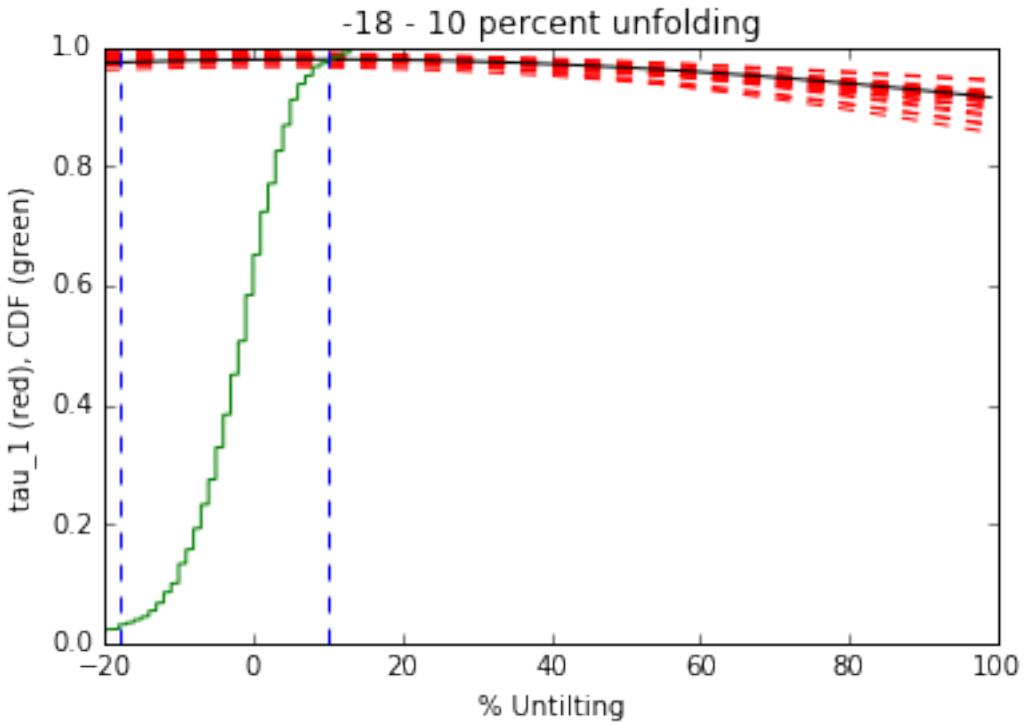

Teel poles summary

```
Out[126]:                      Pole_Lat  Pole_Long      A_95          K        CSD   N  \
          Teel_magnetite_tc -36.495314  16.038788  5.236274  34.392364  13.811918  23
          Teel_hematite_tc  -39.717588  91.918678  7.536314  22.013320  17.264033  18
          Teel_hematite_geo -40.795648  89.426839  5.608638  38.960325  12.976983  18

                                     r   Paleolat
          Teel_magnetite_tc  22.360323 -19.292649
          Teel_hematite_tc   17.227740   3.063432
          Teel_hematite_geo  17.563659   1.925148
```

1.2 Pole compilation for Siberia, North China, and Mongolian terranes

1.2.1 Import existing paleomagnetic data

Siberia Note that a rotation needs to be applied for relative rotation between Aldan and Anabar blocks before the Devonian Period due to Devonian rifting in the Viljuy Basin near the centre of the craton. Here are two rotations used in the literature: Euler Pole (Lat, Long, rotation)

- (60°N, 120°E, 13°) from Smethurst et al. (1998)
- (60°N, 115°E, 25°) everything pre-Devonian (Evans, 2009)
- (60°N, 120°E, 16°) Cambrian to Early Silurian correction (Cocks and Torsvik, 2007)
- (62°N, 117°E, 20°) pre-Devonian (Pavlov et al. (2008) also used in Powerman et al. (2013))

Most Siberia poles are imported from Cocks and Torsvik (2007) which rotates data from the "southern" Siberia (Aldan) into the northern Siberia (Anabar) reference frame according to Smethurst et al. (1998), which the authors claim brings N and S pre-Devonian poles into the best agreement.

Torsvik et al. (2012) updated their Siberia apparent polar wander path by adding data from Shatsillo et al. (2007) that superceded results from the coeval Lena River sediments (Rodianov et al., 1982; Torsvik et al., 1995). However, there are more results from Siberia that must have been discarded by Cocks and Torsvik (2007) and subsequently by other authors. We discuss these poles later on.

Below we plot the paleomagnetic data compiled by Cocks and Torsvik (2007) for Siberia, shaded according to age.

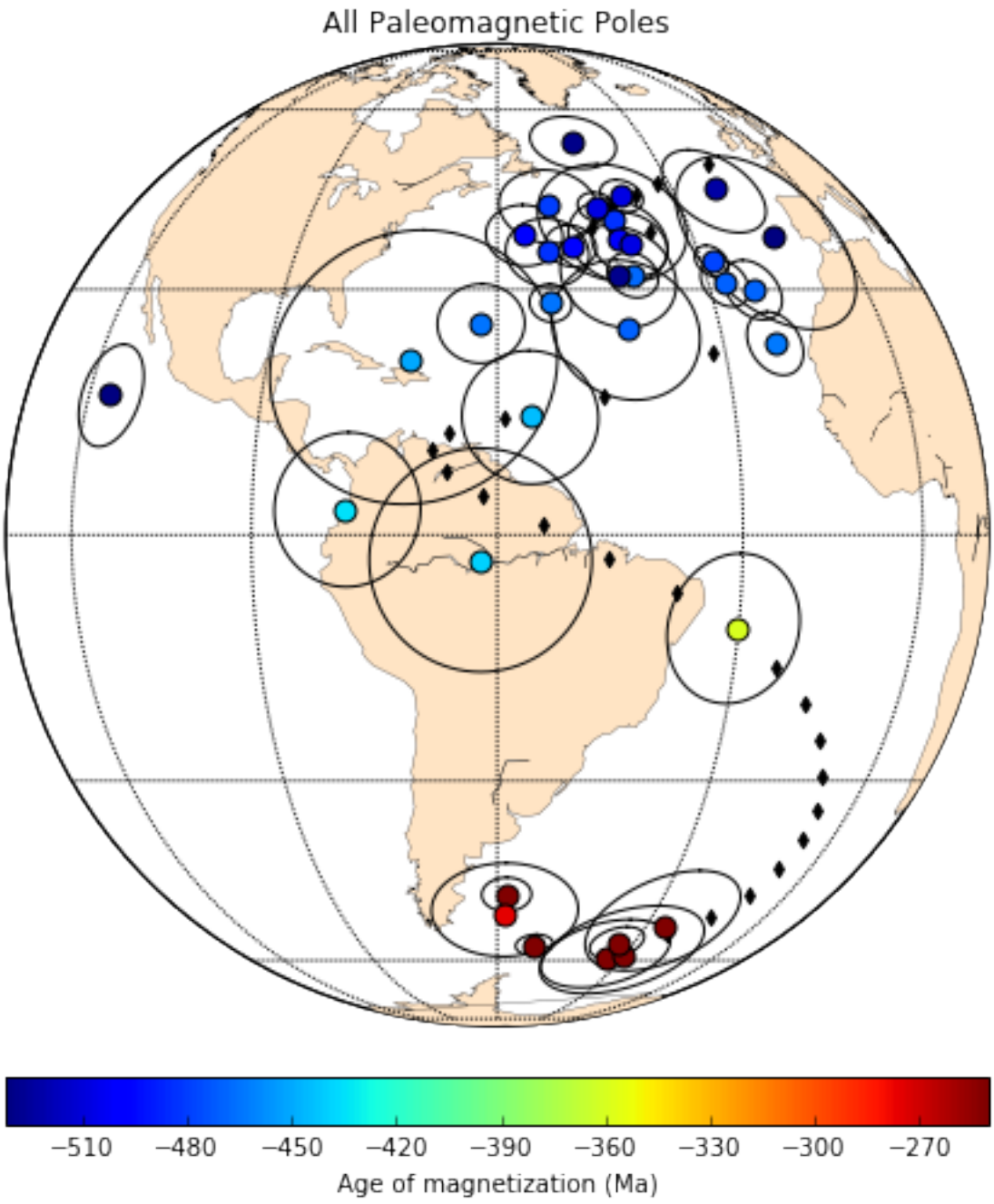

The data from Cocks and Torsvik (2007) are slightly updated by Torsvik et al. (2012) with appropriate euler corrections and evaluation of Ordovician-Silurian poles.

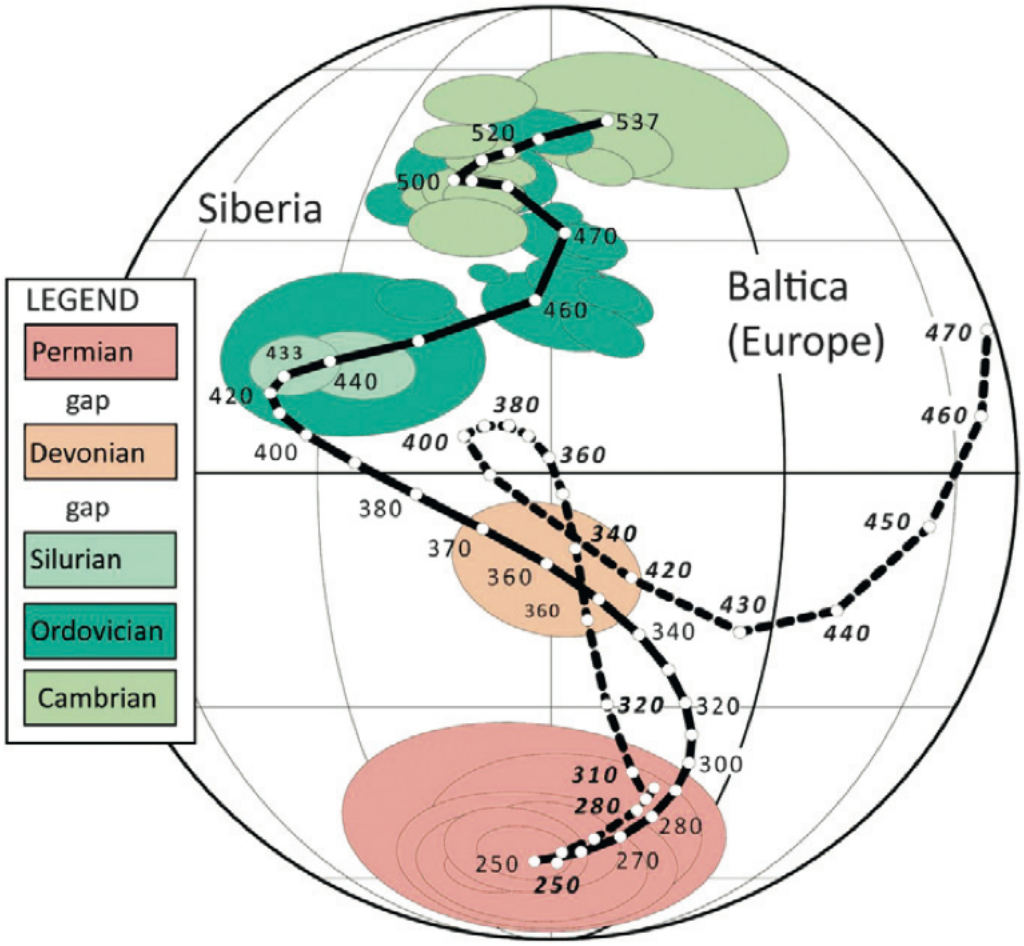

Fig. 12. (a) Revised APWP for Siberia (after Cocks and Torsvik, 2007). Spline path with smoothing parameter of 300 and Q-factor weighted input poles. This path is based on one new Silurian pole (433 Ma; Shatsillo et al., 2007) and elimination of two similar-aged and less reliable poles from Siberia (see text). The Siberian spline path (black thick line) is compared with the spline path for Baltica (Fig. 7a).

In the following analyses, we update this pole list to include additional poles from the area in order to construct a paleolatitdue plot of Siberia through the Phanerozoic Era.

We use the Haversine formula to calculate the distance between the VGPs and a reference point on a given plate. This is then used to calculate the paleolatite of the reference point.

We first load poles for stable Europe from 250 Ma to the present day.

Out[107]:

	high_age	low_age	median_age	A95	PLat	PLon	Paleolat	PLat_N	PLon_N
0	1	0	0.5	3.6	-80.6	267.5	60.638	80.6	87.5
1	1	0	0.5	4.4	-86.4	296.1	55.206	86.4	116.1
2	10	6	8.0	12.9	-84.3	357.7	52.907	84.3	177.7
3	11	8	9.5	1.8	-78.9	328.3	58.733	78.9	148.3
4	11	9	10.0	3.5	-77.4	314.2	61.900	77.4	134.2

Poles from Siberia are then loaded (545 to 250 Ma). Most of the poles were taken from Cocks and Torsvik (2007) and Torsvik et al. (2012), but we also added additional data gathered from the Global Paleomagnetic Database.

Out[146]:

	plate_ID	high_age	low_age	median_age	A95	PLat	PLon	\
0	401	245	243	244.0	10.0	-59.0	330.0	
1	401	258	238	248.0	7.8	-59.3	325.8	
2	401	253	248	251.0	3.3	-56.2	326.0	
3	401	253	248	251.0	9.7	-52.8	334.4	
4	401	253	248	251.0	2.2	-56.6	307.9	
5	401	285	265	275.0	8.6	-50.5	301.4	
6	401	363	290	326.5	1.3	-21.0	350.0	
7	401	352	332	342.0	17.0	-16.0	295.0	
8	401	348	340	344.0	5.8	-25.2	320.0	
9	401	377	350	360.0	8.9	-11.1	329.7	
10	401	377	350	363.5	10.1	-27.8	339.9	
11	401	377	350	363.5	11.9	-22.8	339.4	
12	401	391	363	377.0	5.0	-13.0	302.0	
13	410	430	397	413.5	3.2	8.2	292.0	
14	401	443	423	433.0	4.6	19.0	308.0	
15	410	444	423	433.5	4.4	18.4	302.7	
16	401	454	424	439.0	8.0	14.0	304.0	
17	401	460	440	450.0	17.3	19.4	315.3	
18	410	461	443	452.0	5.1	27.5	332.0	
19	401	464	458	461.0	2.5	22.8	334.2	
20	401	464	458	461.0	5.1	22.1	324.9	
21	401	473	453	463.0	4.0	23.0	338.0	
22	401	470	464	467.0	3.2	30.9	332.7	
23	401	478	458	468.0	3.1	24.4	346.0	
24	401	479	459	469.0	4.0	30.0	337.0	
25	401	480	460	470.0	9.0	17.9	342.8	
26	401	488	468	478.0	2.2	33.9	331.7	
27	401	495	470	482.5	5.8	36.2	338.8	
28	401	493	473	483.0	9.0	40.0	318.0	
29	401	495	485	490.0	4.9	35.2	307.2	
30	401	495	485	490.0	2.3	41.9	315.8	
31	401	510	490	500.0	6.0	37.0	318.0	
32	401	505	495	500.0	3.0	36.1	310.7	
33	401	518	495	506.5	4.5	32.6	333.8	
34	401	514	500	507.0	2.6	43.7	320.5	
35	401	518	505	511.5	4.6	36.4	319.6	
36	401	520	510	515.0	5.1	53.3	315.0	
37	401	535	518	526.5	6.8	44.8	338.7	
38	401	538	518	528.0	7.0	32.0	317.0	
39	401	545	525	535.0	6.2	16.6	244.5	
40	401	545	535	540.0	12.8	37.6	345.0	

	Reference	Paleolat	PLat_N	\

0	GPDB2832, Gurevitch et al. (1995) from Cocks a...	63.178	59.0
1	Walderhaug et al. (2005) from Cocks and Torsvi...	65.344	59.3
2	Gurevitch et al. (2004) from Cocks and Torsvik...	65.004	56.2
3	GPDB3486, Kravchinsky et al. (2002) from Cocks...	59.477	52.8
4	Pavlov and Gallet (1996) from Cocks and Torsvi...	74.988	56.6
5	Pisarevsky et al. (2006) from Cocks and Torsvi...	78.724	50.5
6	GPDB1991, Davydov and Kravchinsky (1973)	30.794	21.0
7	GPDB1986, Kamysheva (1971)	53.142	16.0
8	GPDB3041, Zhitkov et al. (1994)	51.715	25.2
9	GPDB3486, Kravchinsky et al. (2002) from Cocks...	34.892	11.1
10	GPDB3486, Kravchinsky et al. (2002)	42.021	27.8
11	GPDB3486, Kravchinsky et al. (2002)	38.641	22.8
12	GPDB1997, Kamysheva (1975)	48.523	13.0
13	Powerman et al. (2013)	29.655	-8.2
14	Shatsillo et al. (2007) from Cocks and Torsvik...	16.126	-19.0
15	Powerman et al. (2013)	17.919	-18.4
16	Smethurst et al. (1998) from Cocks and Torsvik...	21.927	-14.0
17	Smethurst et al. (1998) from Cocks and Torsvik...	13.660	-19.4
18	Powerman et al. (2013)	0.109	-27.5
19	GPDB3473, Iosifidi et al. (1999) from Cocks an...	3.312	-22.8
20	GPDB3473, Iosifidi et al. (1999) from Cocks an...	7.787	-22.1
21	Smethurst et al. (1998) from Cocks and Torsvik...	1.413	-23.0
22	GPDB3448 Gallet and Pavlov (1998) from Cocks a...	-3.183	-30.9
23	Smethurst et al. (1998) from Cocks and Torsvik...	-3.645	-24.4
24	Smethurst et al. (1998) from Cocks and Torsvik...	-4.193	-30.0
25	Smethurst et al. (1998) from Cocks and Torsvik...	3.434	-17.9
26	Smethurst et al. (1998) from Cocks and Torsvik...	-5.441	-33.9
27	GPDB3474, Surkis et al. (1999) from Cocks and ...	-10.298	-36.2
28	Smethurst et al. (1998) from Cocks and Torsvik...	-6.498	-40.0
29	GPDB3448, Gallet and Pavlov (1998) from Cocks ...	0.651	-35.2
30	GPDB3192, Pavlov and Gallet (1998) from Cocks ...	-7.711	-41.9
31	Smethurst et al. (1998) from Cocks and Torsvik...	-3.690	-37.0
32	GPDB3192, Pavlov and Gallet (1998) from Cocks ...	-0.974	-36.1
33	GPDB3472, Rodionov et al. (1998) from Cocks an...	-5.123	-32.6
34	GPDB3537, Gallet et al. (2003) from Cocks and ...	-10.622	-43.7
35	GPDB3164, Pisarevsky et al. (1997) from Cocks ...	-3.591	-36.4
36	GPDB3537, Gallet et al. (2003) from Cocks and ...	-18.264	-53.3
37	GPDB3164, Pisarevsky et al. (1997) from Cocks ...	-17.577	-44.8
38	Smethurst et al. (1998) from Cocks and Torsvik...	1.285	-32.0
39	GPDB1627, Kirschvink and Rozanov (1984) from C...	13.732	-16.6
40	GPDB3164, Pisarevsky et al. (1997) from Cocks ...	-14.154	-37.6

	PLon_N
0	150.0
1	145.8
2	146.0
3	154.4
4	127.9

```
5    121.4
6    170.0
7    115.0
8    140.0
9    149.7
10   159.9
11   159.4
12   122.0
13   112.0
14   128.0
15   122.7
16   124.0
17   135.3
18   152.0
19   154.2
20   144.9
21   158.0
22   152.7
23   166.0
24   157.0
25   162.8
26   151.7
27   158.8
28   138.0
29   127.2
30   135.8
31   138.0
32   130.7
33   153.8
34   140.5
35   139.6
36   135.0
37   158.7
38   137.0
39    64.5
40   165.0
```

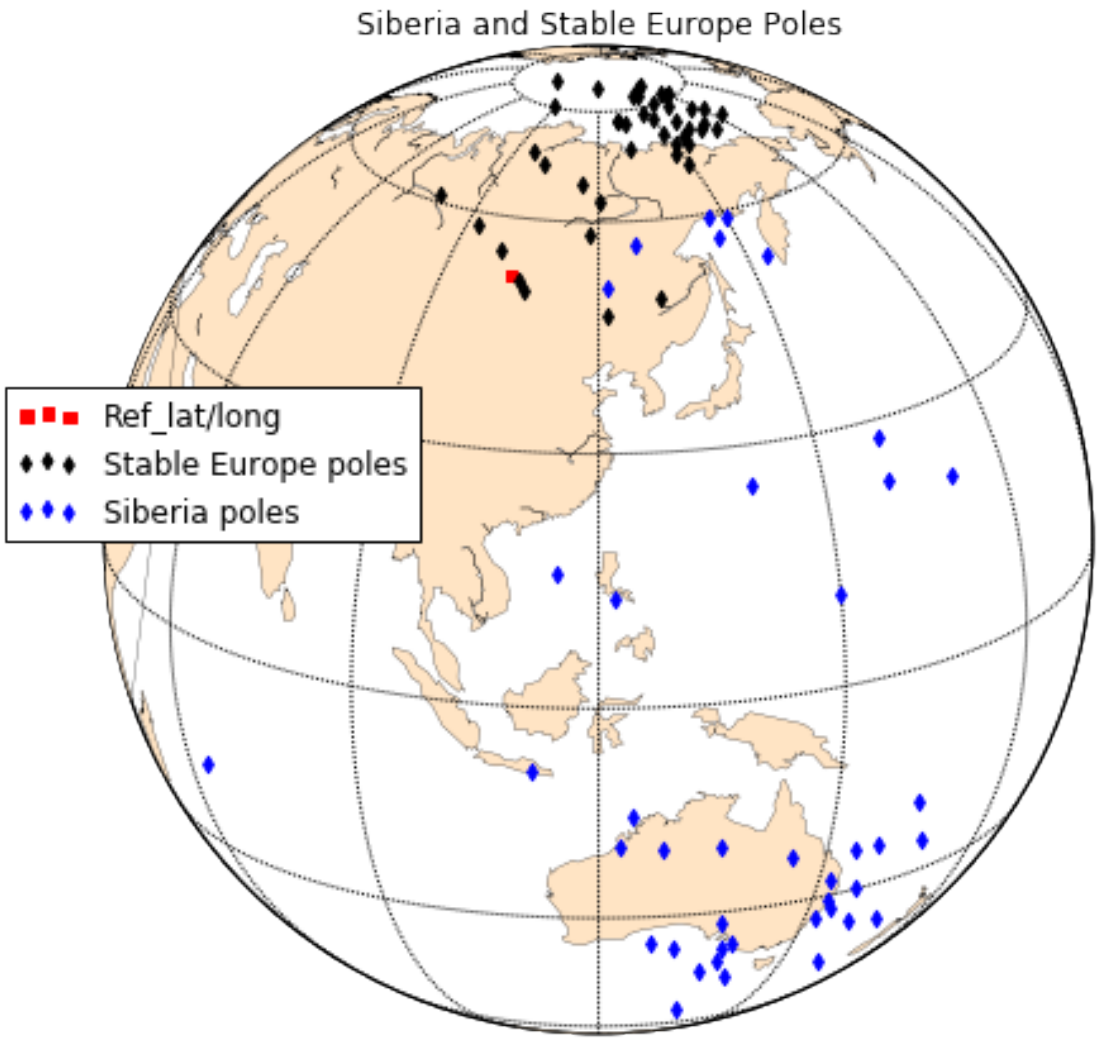

North China We first load the paleomagnetic data for North China compile in Cocks and Torsvik (2013).

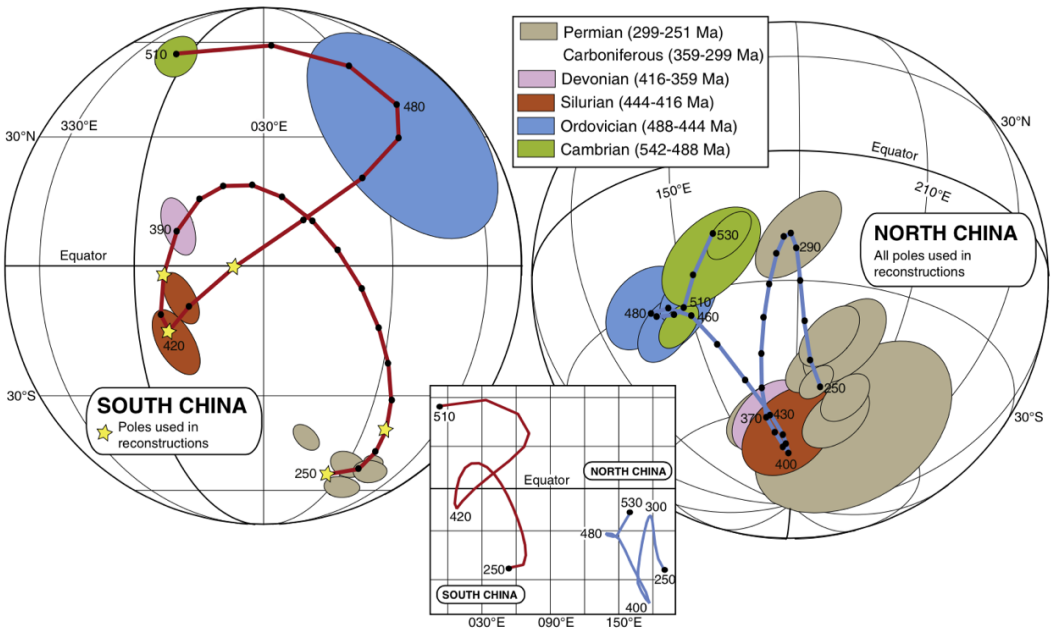

We also add some additional poles from North China that were not included in Cocks and Torsvik (2013) including a compilation of data from Huang et al. (1999) and additional poles from Embleton et al. (1996), Huang et al. (2001), and Doh and Piper (1994).

Out[112]:

	high_age	low_age	median_age	A95	PLat	PLon	References	Paleolat
0	88	68	78	5.8	79.7	170.8	see Van der Voo et al. (2015)	46.149
1	98	78	88	5.3	81.1	294.5	see Van der Voo et al. (2015)	33.136
2	110	90	100	4.7	70.6	156.7	see Van der Voo et al. (2015)	52.870
3	123	103	113	5.2	76.8	192.1	see Van der Voo et al. (2015)	42.209
4	126	106	116	4.6	83.6	172.3	see Van der Voo et al. (2015)	44.602

```
/Users/taylorkilian/Library/Enthought/Canopy_64bit/User/lib/python2.7/site-packages/matplotlib/
  warnings.warn("No labelled objects found. "
```

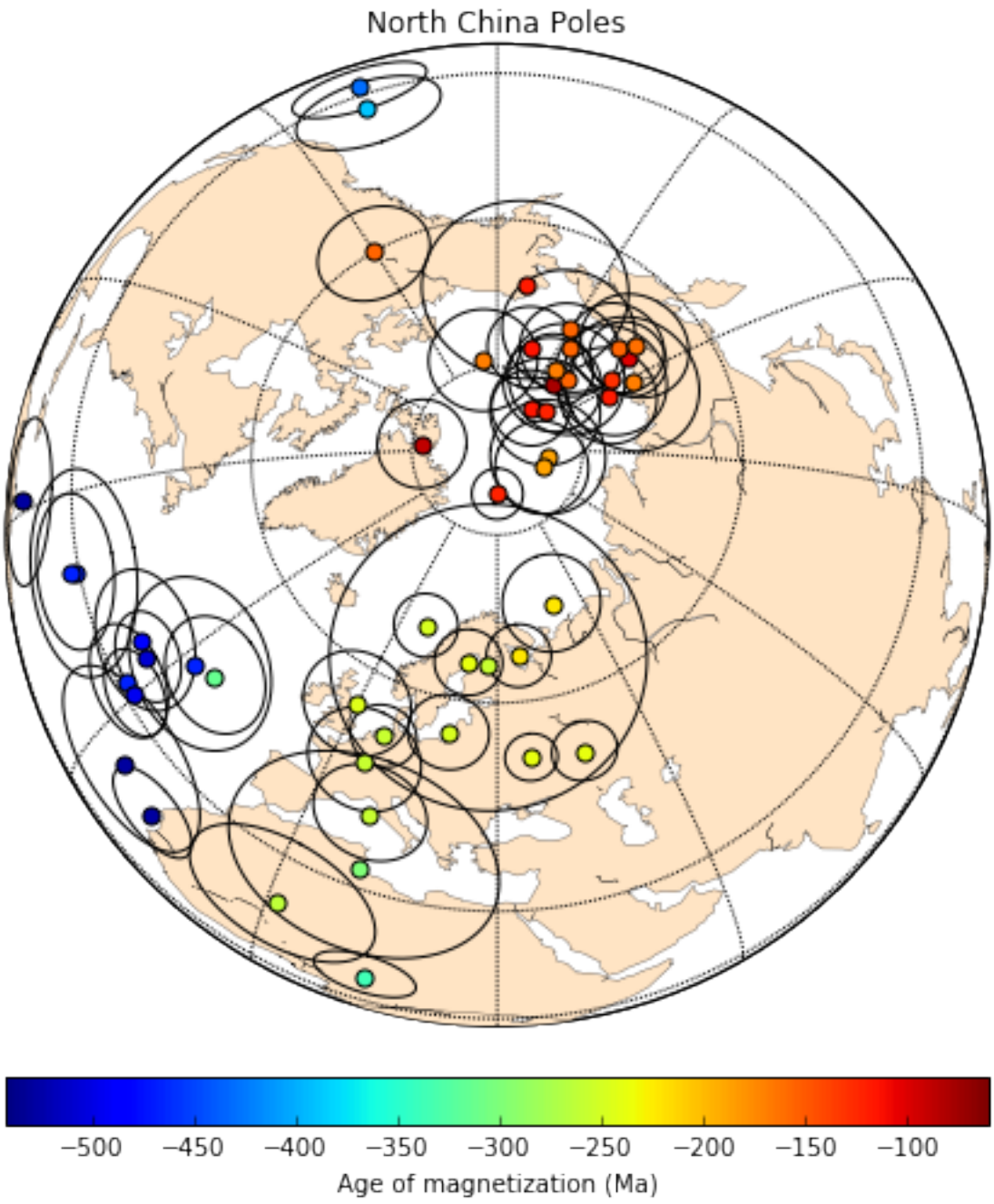

Mongolia pole compilation Edel et al. (2014) published paleomagnetic data from 12 sites in the Trans-Altai and South Gobi zones. This work identified magnetic overprint directions for which a variety of arguments are made as to their temporal relationship. The progression of directions as interpretted by the authors leads to an appreciable change in magnetic declination from overprints intrepretted to be Middle–Late Carboniferous in age to magnetizations that are interpreted to be Permian in age. The authors propose that this declination change is the result of vertical axis

rotation associated with oroclinal bending of a Mongolian ribbon continent (cartoon model shown below).

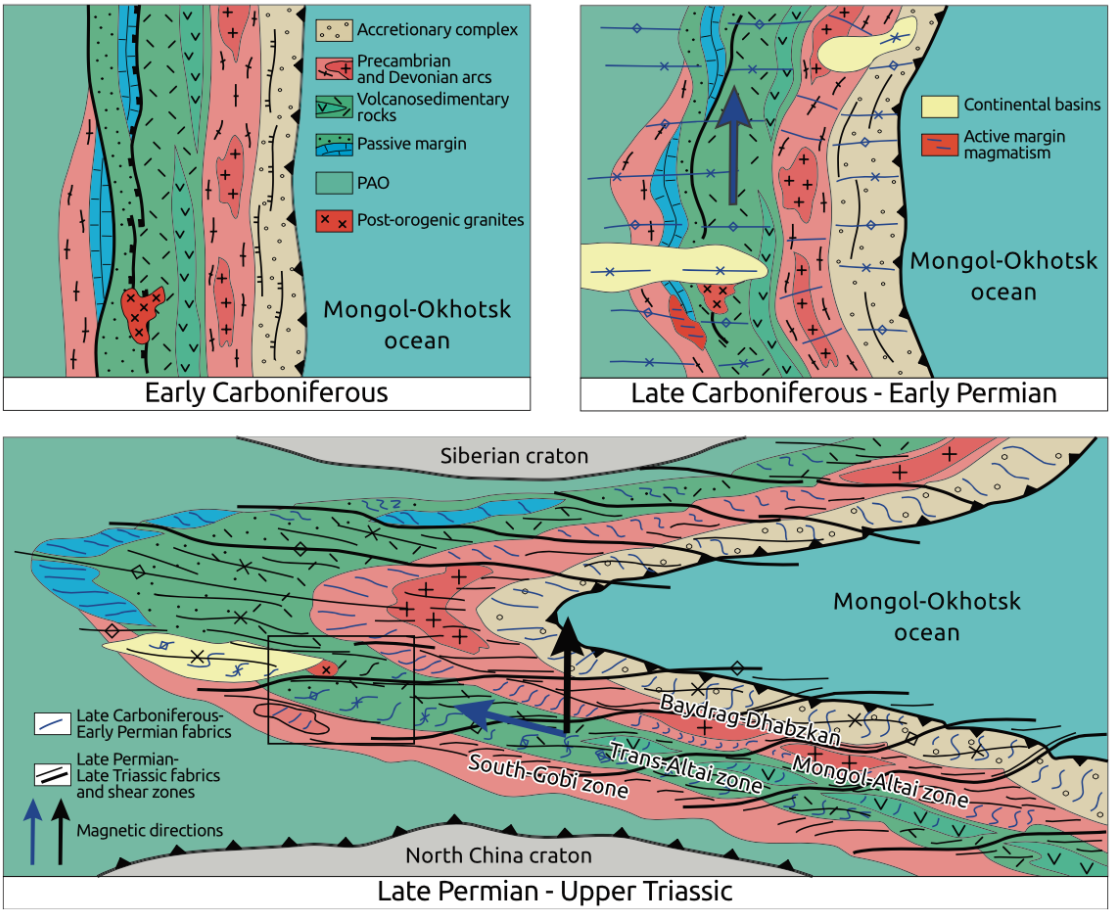

We import paleomagnetic data that have been compiled for Mongolia and some of the surrounding terranes between Siberia and North China and assigned them to established terranes pertinent to this study.

Out[127]:

	terrane	high_age	low_age	median_age	A95	PLat	PLon
0	Zavkhan_Baidrag	105	92	98.5	3.9	81.1	165.7
1	Zavkhan_Baidrag	146	65	105.5	21.4	86.9	252.8
2	Zavkhan_Baidrag	124	92	108.0	2.5	80.8	158.4
3	Zavkhan_Baidrag	119	115	117.0	4.9	75.6	132.3
4	greater_Amuria	130	110	120.0	5.2	70.8	322.4
5	greater_Amuria	145	97	121.0	4.2	58.3	51.0
6	Zavkhan_Baidrag	125	118	121.5	4.3	82.0	172.3
7	greater_Amuria	133	125	129.0	7.4	86.8	61.8
8	greater_Amuria	161	145	153.0	3.1	58.9	327.3
9	greater_Amuria	176	145	160.5	4.2	59.6	279.0
10	greater_Amuria	245	208	226.5	16.8	32.0	32.7

11	southern_terranes	260	228	244.0	8.0	50.0	201.0
12	Zavkhan_Baidrag	260	240	250.0	11.0	55.0	131.3
13	greater_Amuria	271	260	265.5	14.4	63.1	151.0
14	greater_Amuria	290	256	273.0	11.6	44.8	335.1
15	southern_terranes	310	245	277.5	8.0	46.0	273.0
16	southern_terranes	300	280	290.0	7.8	71.0	188.0
17	Zavkhan_Baidrag	323	290	306.5	10.4	37.5	320.1
18	southern_terranes	363	323	343.0	13.0	-1.0	354.1
19	southern_terranes	391	363	377.0	3.4	39.9	244.3
20	southern_terranes	391	363	377.0	4.6	51.7	282.7
21	southern_terranes	391	363	377.0	3.5	38.0	244.0
22	southern_terranes	391	363	377.0	5.1	52.0	280.0
23	southern_terranes	363	245	304.0	11.9	50.0	354.0
24	southern_terranes	340	299	319.5	13.0	5.0	341.0
25	Zavkhan_Baidrag	440	200	320.0	5.6	40.8	269.4
26	southern_terranes	360	320	340.0	4.9	10.0	330.0
27	Lake_Zone	423	397	410.0	5.8	-13.3	63.7
28	Lake_Zone	428	397	412.5	6.1	26.3	144.0
29	Lake_Zone	428	416	422.0	3.6	-17.5	100.1
30	Zavkhan_Baidrag	450	410	430.0	12.3	7.0	106.7
31	Zavkhan_Baidrag	449	443	446.0	5.2	36.5	196.0
32	Zavkhan_Baidrag	542	360	451.0	4.6	3.5	114.9
33	Zavkhan_Baidrag	545	518	531.5	13.5	21.4	347.1
34	Zavkhan_Baidrag	545	518	531.5	10.1	14.7	228.6
35	Zavkhan_Baidrag	545	518	531.5	4.4	24.1	283.3
36	Zavkhan_Baidrag	650	518	584.0	4.7	17.6	309.7
37	Zavkhan_Baidrag	650	518	584.0	5.4	22.6	285.6

	Reference	Paleolat
0	van Hinsbergen et al. (2008)	49.393
1	GPDB2443, Pruner (1992)	44.225
2	van Hinsbergen et al. (2008)	50.579
3	van Hinsbergen et al. (2008)	57.658
4	Cogne et al. (2005)	32.628
5	Halim et al. (1998)	61.511
6	van Hinsbergen et al. (2008)	48.319
7	Cogne et al. (2005)	49.735
8	Cogne et al. (2005)	24.229
9	Kravchinsky et al. (2002)	16.741
10	GPDB2443, Pruner (1992)	40.779
11	Edel et al. (2014)	26.317
12	Kovalenko (2010)	66.385
13	Kravchinsky et al. (2002)	55.811
14	GPDB2443, Pruner (1992)	15.820
15	Edel et al. (2014)	3.123
16	Kovalenko (2010)	43.039
17	GPDB2443, Pruner (1992)	3.567
18	GPDB3045, Pechersky and Didenko (1995)	-8.390

19	GPDB3045, Pechersky and Didenko (1995)	1.297
20	GPDB3045, Pechersky and Didenko (1995)	8.999
21	GPDB2594, Grishin et al. (1991)	-0.399
22	GPDB2594, Grishin et al. (1991)	9.179
23	GPDB2594, Grishin et al. (1991)	28.348
24	Edel et al. (2014)	-12.479
25	This study	-1.939
26	Kovalenko (2010)	-15.126
27	Bachtadse et al. (2000)	23.280
28	Bachtadse et al. (2000)	46.717
29	Bachtadse et al. (2000)	25.260
30	Kravchinsky (2010)	48.745
31	This study	19.566
32	Evans et al. (1996)	43.245
33	Kravchinsky (2001)	3.927
34	GPDB3045, Pechersky and Didenko (1995)	-15.368
35	GPDB3045, Pechersky and Didenko (1995)	-18.442
36	GPDB3045, Pechersky and Didenko (1995)	-18.324
37	GPDB3045, Pechersky and Didenko (1995)	-19.692

Calculate paleolatitudes for the Mongolia poles, considering that many may have experienced horizonatal-axis rotations during the formation of the COAB and possibly earlier.

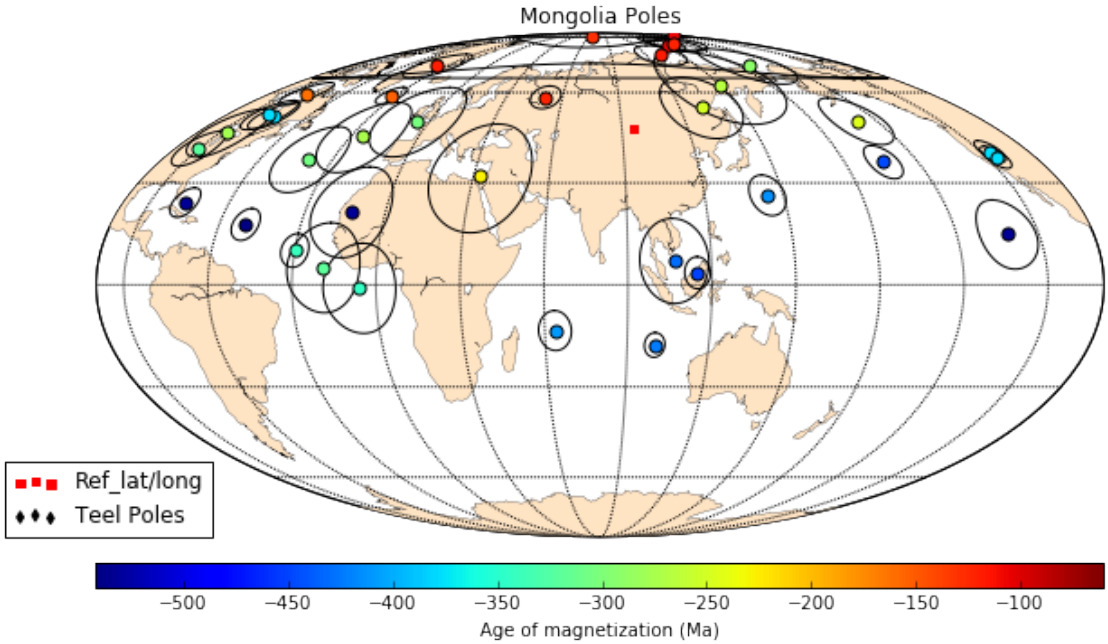

1.3 Paleolatitude diagram

We plot the data plot all of the data from Siberia, North China, and Monogolia (from Zavkhan, Baidrag, Lake Zone, and other southern terranes) on a paleolatitude v. time plot. The paleolati-

tudes given for each block are for specific reference points on each terrane. For Mongolia, the site of the Teel Formation is used (95.38 °N, 47.1 °E). For Siberia, coordinates at the southern tip of the craton (51.7 °N, 103.5 °E) are given seeing as this would be the proposed conjugate margin for Mongolia. For north China, a reference point on the northern margin (42 °N, 109 °E) is given to represent the an alternative conjugate margin that would have shared very similar paleolatitudes with Mongolia if they were attached.

There are a handful of Mongolian poles that we exclude because of wide age uncertainties or lack of statistical robustness. The Bachtadse et al. (2000) component B pole is dismissed because of the small number or samples used to calculate the mean direction (25 samples; unblocking temperatures of 270–420 °C); it is very similar to two Levashova (2010) directions which may be overprints (see below). The Evans et al. (1996) Bayan-Gol pole was superceded by results from Kravchinsky (2001) and may likely be a pre-folding overprint, given the increase in precision after tilt correction. The Kravchinsky et al. (2010) pole, that they call a remagnetization, has a very uncertain age and is not tilt-corrected, therefore we see it as unreliable for a paleolatitude estimate. The Kovalenko (2010) pole from the granite at Hanbogd is excluded because it is only from one site and is in the Trans-Altai zone, which is severely affected by early Triassic deformation along the Gobi-Tienshan fault (Lehmann et al., 2010). The "Mongolian sediments and volcanics, Gurvan-Sayhan Range, post-folding" pole from Grishin et al. (1991) (also discussed in Pechersky and Didenko (1995)) is dismissed because it is likely underaveraged (only from one site) and because of its large age uncertainty; it is also a post-folding remanence.

```
<matplotlib.figure.Figure at 0x116988d90>
```

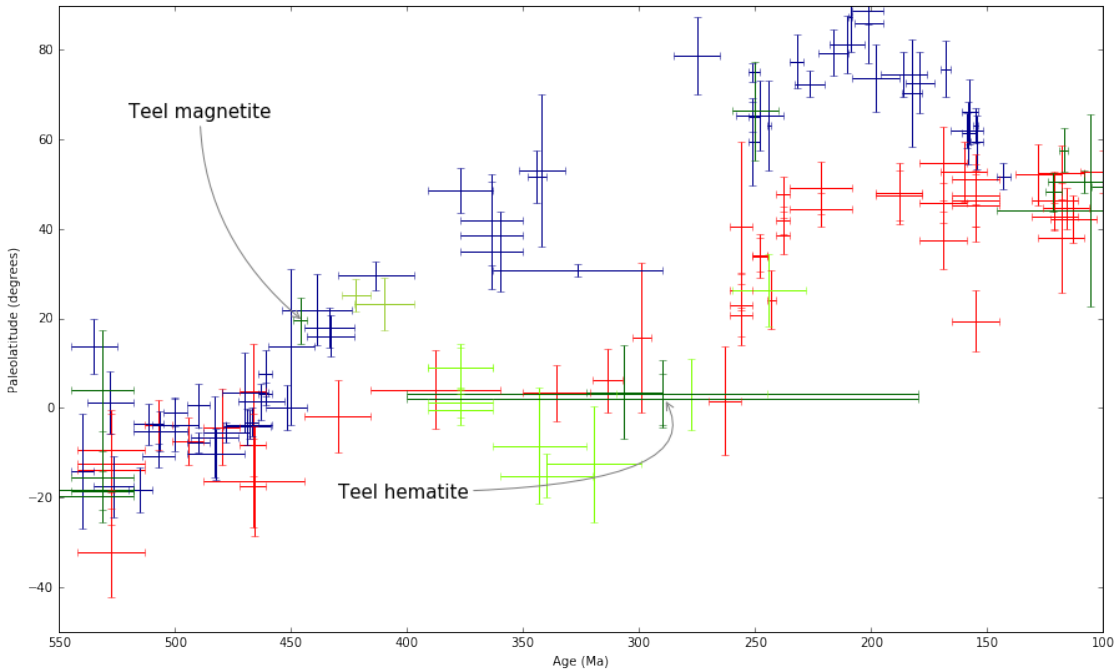

1.4 Regional overprints in Precambrian rocks

In order to understand the regional paleomagnetic directions, specifically possible overprints, we compare results from the Zavkhan block to see if there are dominant overprints that affected all rocks. These results are from Levashova et al. (2010), Kravchinsky et al. (2001), Evans et al. (1996), this study, and preliminary data from the Zavkhan volcanics.

Out[135]:

	ID	N	k_geo	Dec_geo	Inc_geo	a95_geo	k_tc	Dec_tc	Inc_tc	a95_tc	comments
0	Lev10-INT	18	19.0	272.8	-66.2	8.2	3.0	158.7	-42.8	24.7	NaN
1	Lev10-HT	11	3.0	311.7	-11.0	30.1	19.0	321.9	-65.0	10.7	NaN
2	Lev11-INT	27	14.0	207.9	-30.6	7.8	6.0	210.4	-4.0	12.4	NaN
3	Lev11-HT	18	10.0	194.2	29.2	11.5	41.0	179.6	53.7	5.4	NaN
4	Krav01-LOW	10	59.7	4.1	70.9	6.3	96.8	181.2	85.6	4.9	data from both B-G and T-O
5	Krav01-INT	9	31.3	209.2	-66.0	9.3	117.6	284.3	-79.7	4.8	data from both B-G and T-O
6	Krav01-HT	6	14.9	118.5	5.3	17.9	13.3	118.3	-6.3	19.0	data from B-G
7	Teel_mag	23	29.1	186.6	-64.9	5.7	38.5	236.6	-35.0	4.9	NaN
8	Teel_hem	18	14.9	184.6	3.8	9.3	14.2	182.9	6.1	9.5	NaN
9	Evans_HT	193	NaN	NaN	NaN	NaN	5.8	331.9	-62.6	4.6	NaN
10	Z09_cgl_INT	20	32.3	200.7	-62.2	5.8	32.3	212.3	-5.8	5.8	NaN
11	Z104_cgl_INT	31	165.4	174.8	-61.7	2.0	165.2	61.9	-71.4	2.0	NaN

All directions are first plotted in geographic coordinates.

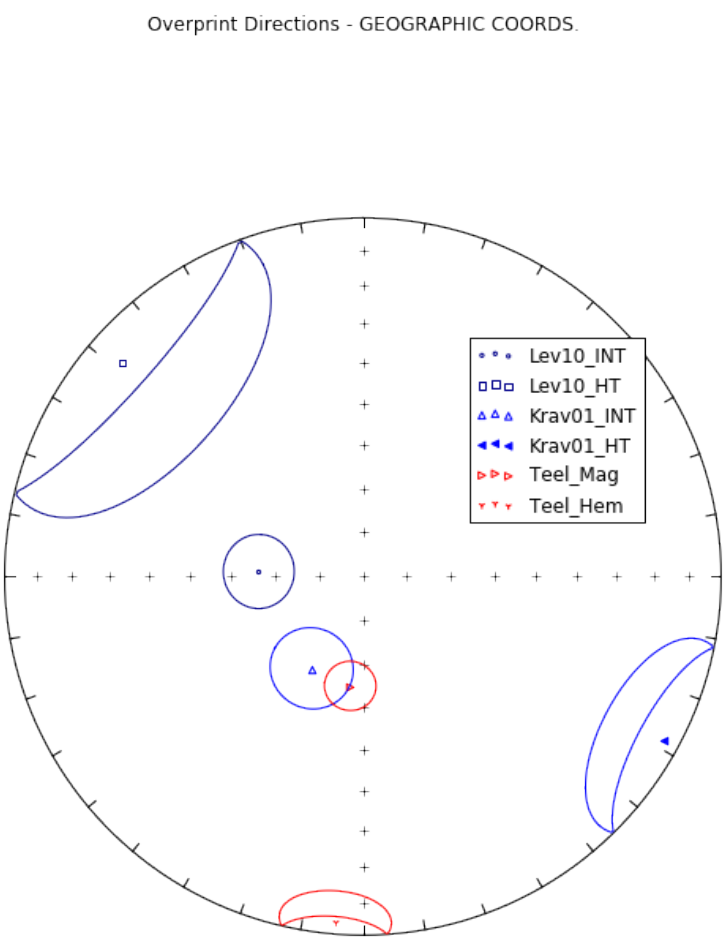

Then the overprint data are plotted in tilt-corrected coordinates.

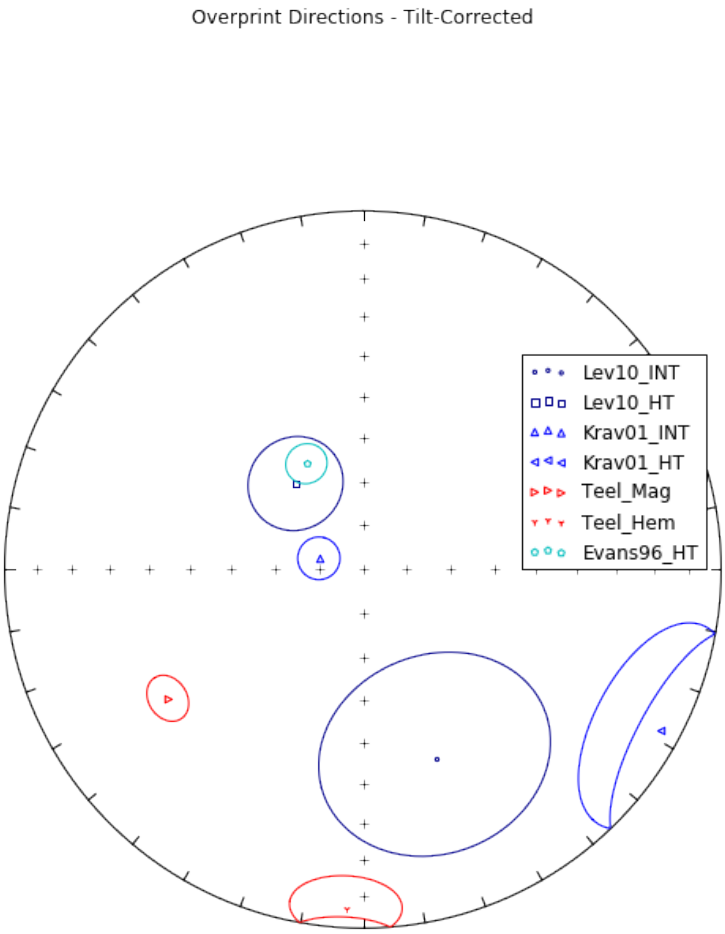

Given geological and statistical paleomagnetic context (improvement during tilt correction) we creat a plot of what we believe to be the actual overprint direction if they were acquired either before or after folding.

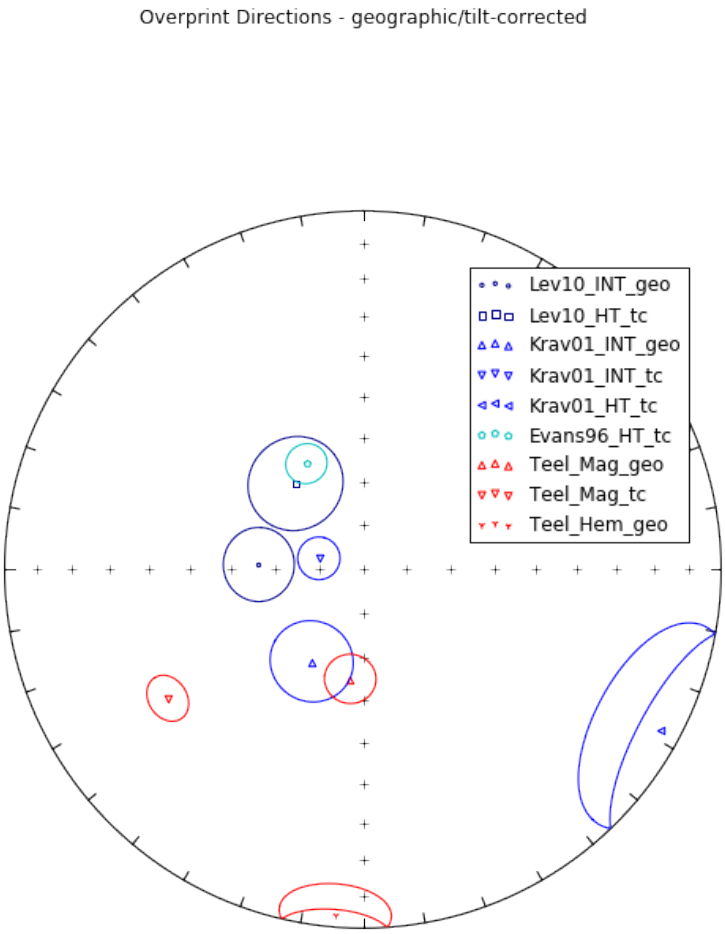

As stated in the main text, the Kravchinsky et al. (2001) intermediate component in geographic coordinates is similar to the Teel magnetite component in geographic coordinates. This similarity may be meaningless because the intermediate component of Kravshinsky et al. (2001) improves in precision after tilt-correction. This argues for the primary nature of the tilt-corrected Teel magnetite component, or rather that this componenet was acquired before folding/tilting of bedding.

1.5 Additional References

Bachtadse, V., Pavlov, V. E., Kazansky, A. Y., and Tait, J. A., 2000, Siluro-Devonian paleomagnetic results from the Tuva Terrane (southern Siberia, Russia): implications for the paleogeography of Siberia: Journal of Geophysical Research: Solid Earth, vol. 105, pp. 13,509-13,518, doi:10.1029/1999JB900429.

Cogne, J.-P., Kravchinsky, V. A., Halim, N., and Hankard, F., 2005, Late Jurassic-Early Cretaceous closure of the Mongol-Okhotsk Ocean demonstrated by new Mesozoic palaeomagnetic results

from the Trans-Baikal area (SE Siberia): Geophysical Journal International, vol. 163, pp. 813-832, doi:10.1111/j.1365-246X.2005.02782.x.

Edel, J. B., Schulmann, K., Hanzl, P., and Lexa, O., 2014, Palaeomagnetic and structural constraints on 90° anticlockwise rotation in SW Mongolia during the Permo-Triassic: Implications for Altaid oroclinal bending. Preliminary palaeomagnetic results: Journal of Asian Earth Sciences, vol. 94, pp. 157-171, doi:10.1016/j.jseaes.2014.07.039.

Evans, D. A., Zhuravlev, A. Y., Budney, C. J., and Kirschvink, J. L., 1996, Palaeomagnetism of the Bayan Gol Formation, western Mongolia: Geological Magazine, vol. 133, pp. 487-496.

Grishin, D., Didenko, A., Pechersky, D., and T.L., T., 1991, [Paleomagnetic study and petromagnetic study of structure and evolution of paleooceanic lithosphere (Phanerozoic ophiolites of Asia)] (in Russian), VNIGRI, Leningrad, Russia, pp. 135-149.

Halim, N., Kravchinsky, V., Gilder, S., Cogne, J.-P., Alexyutin, M., Sorokin, A., Courtillot, V., and Chen, Y., 1998, A palaeomagnetic study from the Mongol-Okhotsk region: rotated Early Cretaceous volcanics and remagnetized Mesozoic sediments: Earth and Planetary Science Letters, vol. 159, pp. 133-145, doi:10.1016/S0012-821X(98)00072-7.

Kovalenko, D., 2010, Paleomagnetism of Late Paleozoic, Mesozoic, and Cenozoic rocks in Mongolia: Russian Geology and Geophysics, vol. 51, pp. 387-403, doi:10.1016/j.rgg.2010.03.006.

Kravchinsky, V., Konstantinov, K., and Conge, J., 2001, Palaeomagnetic study of Vendian and Early Cambrian rocks of South Siberia and Central Mongolia: Was the Siberian platform assembled at this time?: Precambrian Research, vol. 110, pp. 61-92.

Kravchinsky, V. A., Cogne, J.-P., Harbert, W. P., and Kuzmin, M. I., 2002, Evolution of the Mongol-Okhotsk Ocean as constrained by new palaeomagnetic data from the Mongol-Okhotsk suture zone, Siberia: Geophysical Journal International, vol. 148, pp. 34-57.

Kravchinsky, V. A., Sklyarov, E. V., Gladkochub, D. P., and Harbert, W. P., 2010, Paleomagnetism of the Precambrian Eastern Sayan rocks: Implications for the Ediacaran-Early Cambrian paleogeography of the Tuva-Mongolian composite terrane: Tectonophysics, vol. 486, pp. 65-80, doi:10.1016/j.tecto.2010.02.010.

Pechersky, D. and Didenko, A., 1995, Paleo-Asian Ocean (in Russian): United Institute of Earth's Physics Publ., Moscow, 298 pp.

Pruner, P., 1992, Palaeomagnetism and palaeogeography of Mongolia from the Carboniferous to the Cretaceous - final report: Physics of the Earth and Planetary Interiors, vol. 70, pp. 169-177, doi:10.1016/0031-9201(92)90179-Y.

Van Hinsbergen, D. J. J., Straathof, G. B., Kuiper, K. F., Cunningham, W. D., and Wijbrans, J., 2008, No vertical axis rotations during Neogene transpressional orogeny in the NE Gobi Altai: coinciding Mongolian and Eurasian early Cretaceous apparent polar wander paths: Geophysical Journal International, vol. 173, pp. 105-126, doi:10.1111/j.1365-246X.2007.03712.x.